22

30.05.99

ISRAELI FEL TWO-STAGE COLLECTOR SIMULATIONS

Sergey Efimov

1. INTRODUCTION

The beam dynamics problem in the region after deceleration is to collect a low-energy beam with an energy spread of about 7% in the wiggler region at the collector. The energy spread due to radiation in the wiggler was calculated for the Israeli Free Electron Laser (FEL) based on the FEL 3D simulation program and is described in [1]. Measurements of collected current in the different parts of the collector for various potentials enable one to obtain information on beam energy spread, using the collector as a spectrometer.

The layout of this part of the Israeli FEL [2] is shown on the Fig.1. Our two-stage collector consists of two parts: A "Collector tube 1" (CT1) and a "Collector tube 2" (CT2). The length of CT1 is 1500mm. It contacts the 10-th electrode (numbers of electrodes start from the decelerator exit, i.e. from right to left on this picture) of the decelerator. Its potential equals 75kV with respect to ground (or 118kV with respect to the electron gun cathode). Using an independent voltage supply, the potential of the CT1 can be varied in range of 40kV to 80kV in respect to ground. The range of these potentials is limited by onset of sparking between electrodes of the decelerator. Length of CT2 is 850mm and its potential can be changed from -80kV up to 80kV in respect to ground. The distance between CT1 and CT2 is 132mm, the gate valve is disposed on this space. Short solenoids C5 and C6 are not used in this scheme of the collector.

The goal of this work is to simulate the beam distribution in the two-stage collector for different potentials including secondary electron effects, to determine efficiency of beam collection for this design and to obtain data for comparison with experiments.

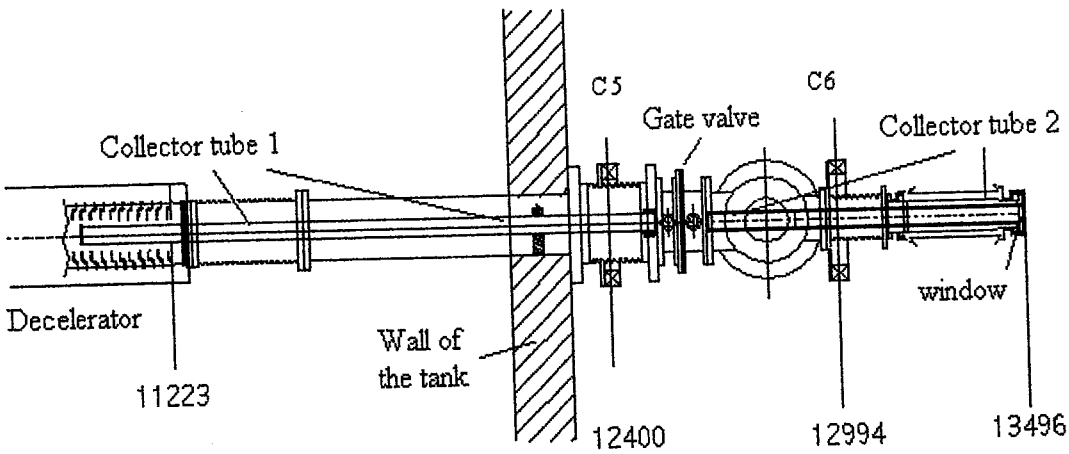

Fig.1. Structure of the two-stage collector. Numbers below are the distances of elements from the electron gun cathode. C5, C6 - short focusing solenoids.

1. INITIAL BEAM PARAMETERS.

Initial ray position in the phase space (r, r') and its numbers (from 1 to 48 and from 529 to 536) in the input file for beam energy E=1.32MeV (56rays) are shown on the Fig.2. r_i is the radial coordinate of the i -ray, $r'_i=\partial r_i/\partial z$ and it is proportional to transverse impulse of the i -ray. There is beam energy distribution on the entrance of the decelerator tube below this picture. The beam equilibrium kinetic energy 1.4MeV is marked by the needle and corresponds to case without radiation. The range of beam energy is 1.32-1.42MeV with step 0.01MeV and a full number of the rays for simulations is 56*11=616. Beam current is I=1A. Initial beam emittance is 22π mm*mrad and beam radius is 10mm. Groups of rays with equal energies are

designated by numbers I-XI (11groups). Uniform current density distribution is used.

For simulations EGUN code [3] was used.

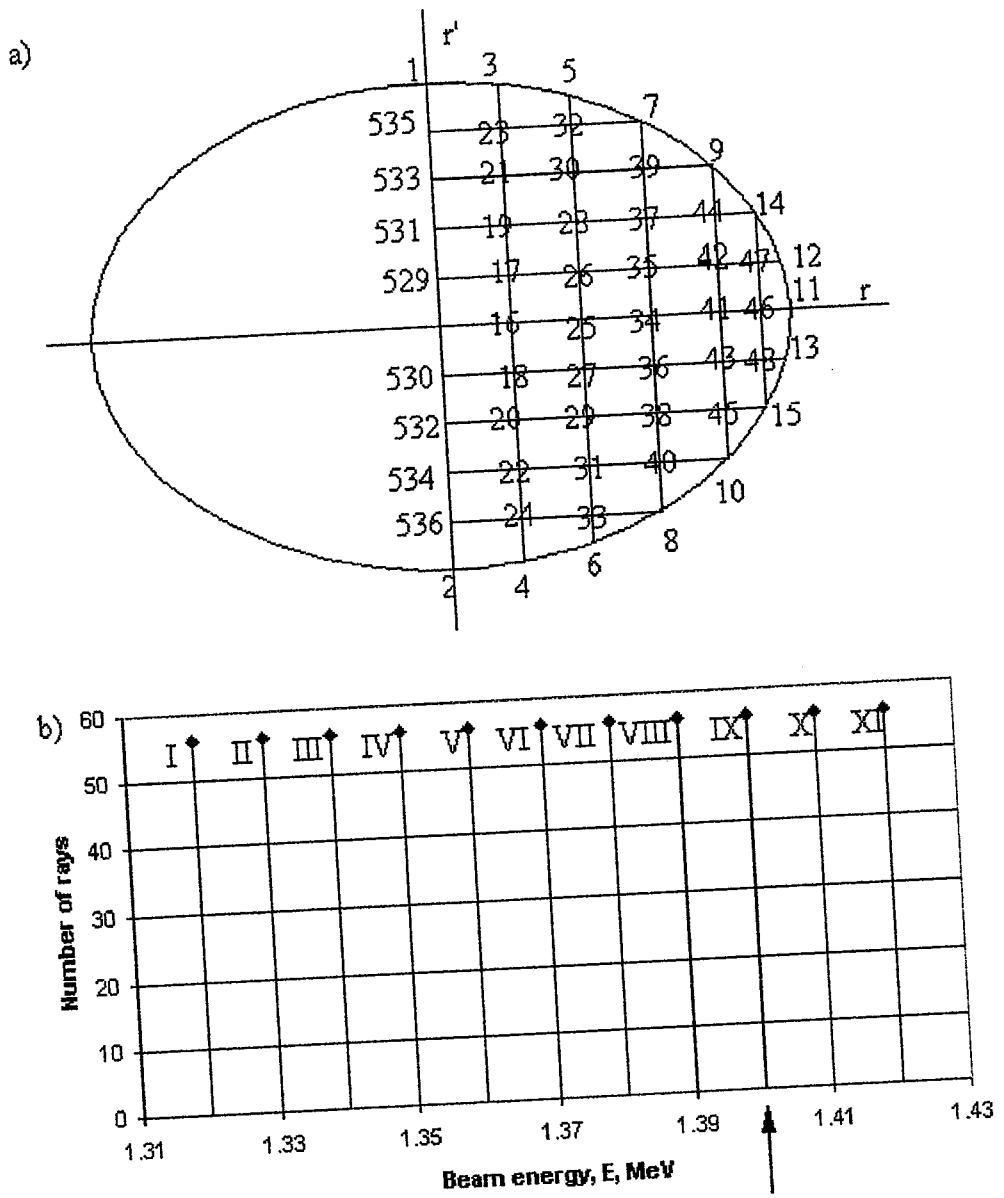

Fig. 2. Initial beam rays in the phase space (a) and their energy composition (b).

2. RESULTS OF SIMULATIONS.

2.1. PRIME BEAM.

The simulated structure is submitted as consisting from 2 parts. Beam tracing across the first part and its form on the phase space are shown on the Fig.3.

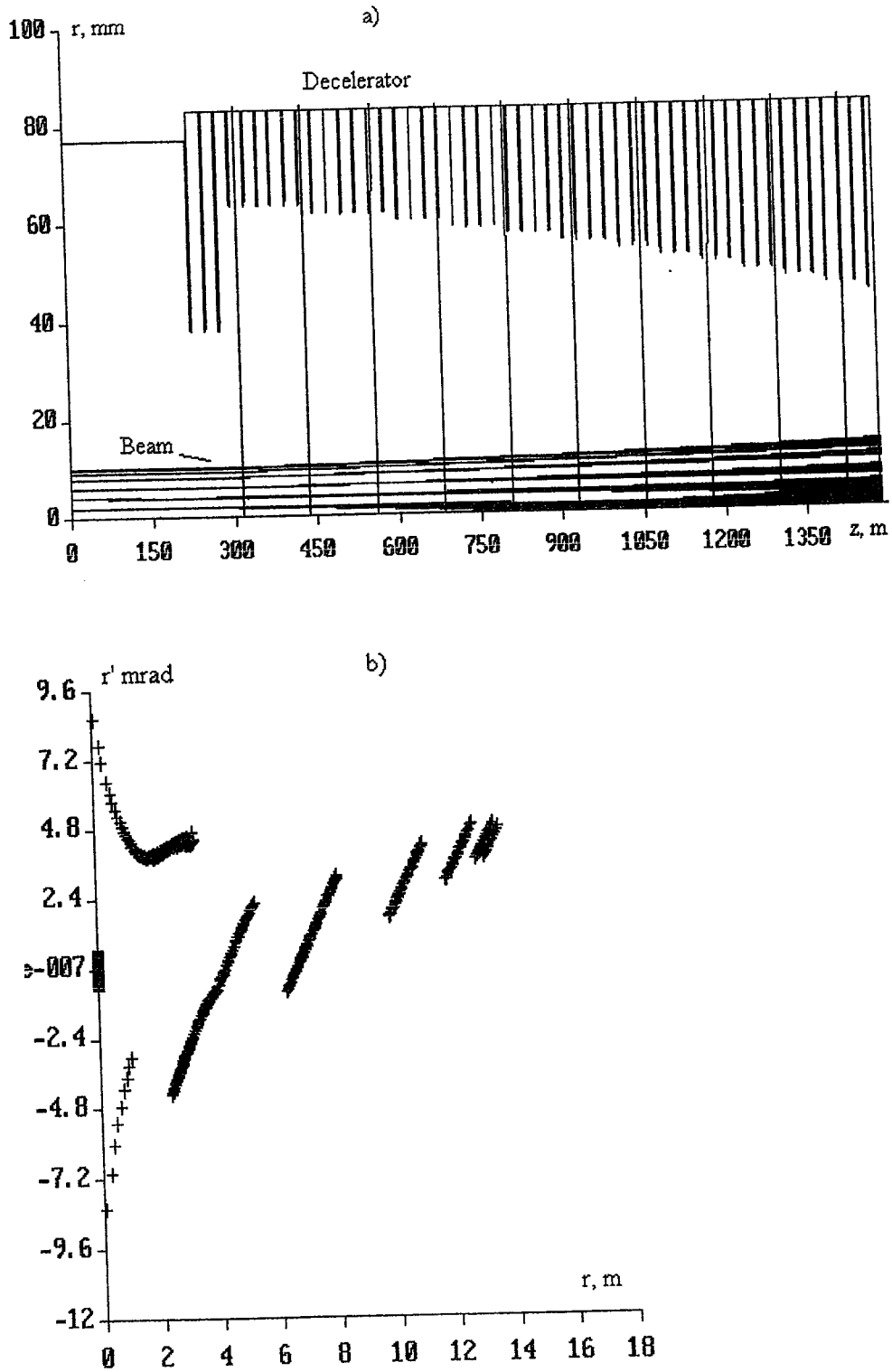

Fig. 3. Beam tracing on the first part of the decelerator (a) and rays on the phase space after the first part of the decelerator (b).

There is the following information on Fig. 4: beam tracing up to the entrance of the two-stage collector, geometry of this collector, beam energy composition after the decelerator (on the CT1 entrance). Potential of the CT1 relatively to the electron gun cathode is equal to 118kV (correspondingly 118keV equilibrium beam energy is marked by needle on the picture). Groups of rays with equal energies in the initial beam are designated by numbers I-XI (11groups).

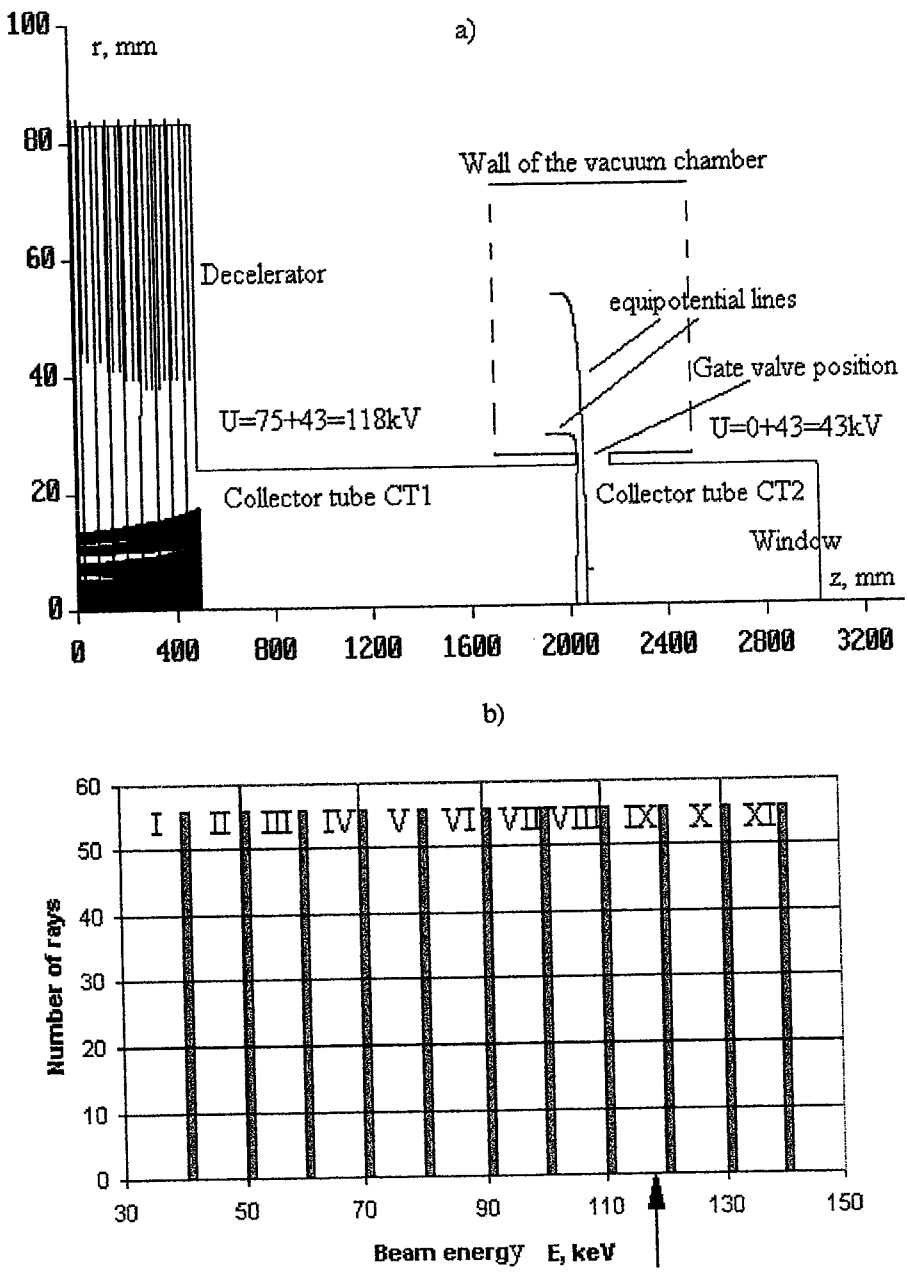

Fig.4. Beam on the enter of the CT1 (a) and its energy composition (b).

Two main groups of simulations for different means of potentials CT1 and CT2 were done: beam dynamic simulations for prime beam only and prime beam dynamics together with secondary electron effects. These results of beam dynamic are located in Appendix I and Appendix II correspondingly. Pictures of the Appendix I (Fig. 18 - Fig.32) illustrate prime beam tracing and longitudinal distribution of the collection beam in the collector for different potentials of the CT1 and CT2. Total current for case U(CT1)=40kV and for U(CT2) varied are shown on the Tab.1 and Fig.5 (this results were taken from the Appendix I Fig.18-Fig.22). Difference between full initial beam current 1A and total beam collection in the CT1, the CT2, and the window determinate beam losses in the gate valve region. It's possible to see that increasing of the CT2 potential more then 15kV almost don't influence the distribution of the beam collections in longitudinal direction.

Table 1.

U(CT2), kV	I(CT1), mA	I(CT2), mA	I(Window), mA	I(CT2)+I(Window), mA
-60	893	39	16	55
-40	803	59	104	163
0	641	29	323	352
40	617	39	344	383
60	615	50	335	385

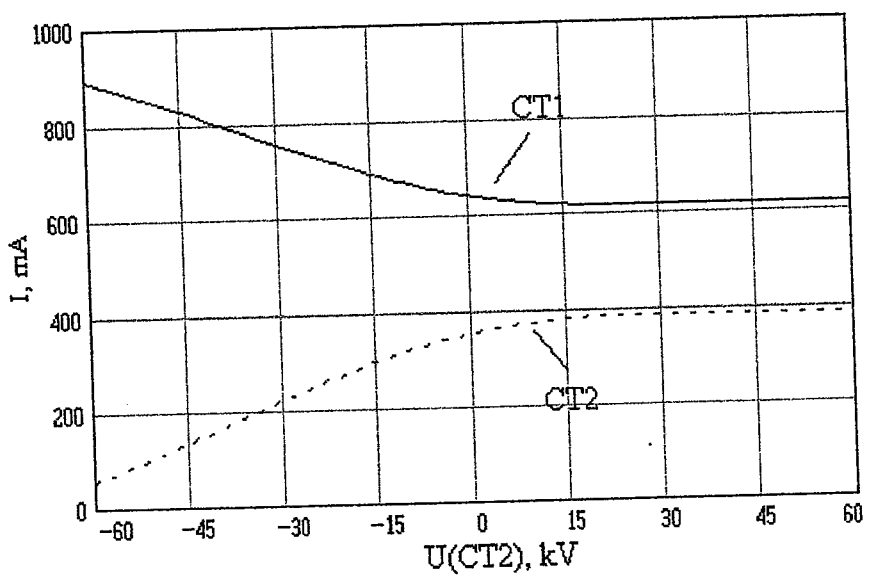

Fig.5. Current of the beam collection on CT1 (above) and CT2 + Window (below) versus potential of the CT2 for U(CT1)=40kV. Total beam current is 1A.

Total results for case if U(CT1)=60kV and U(CT2) varied are shown on the Tab.2 and Fig.6. Details of beam dynamics in this case it can see in the Appendix I (Fig.23-Fig.27).

Table 2

U(CT2), kV	I(CT1), mA	I(CT2), mA	I(Window), mA	I(CT2)+I(Window), mA
-60	862	39	16	55
-40	781	91	75	116
0	623	65	310	375
40	570	92	336	428
60	570	101	329	430

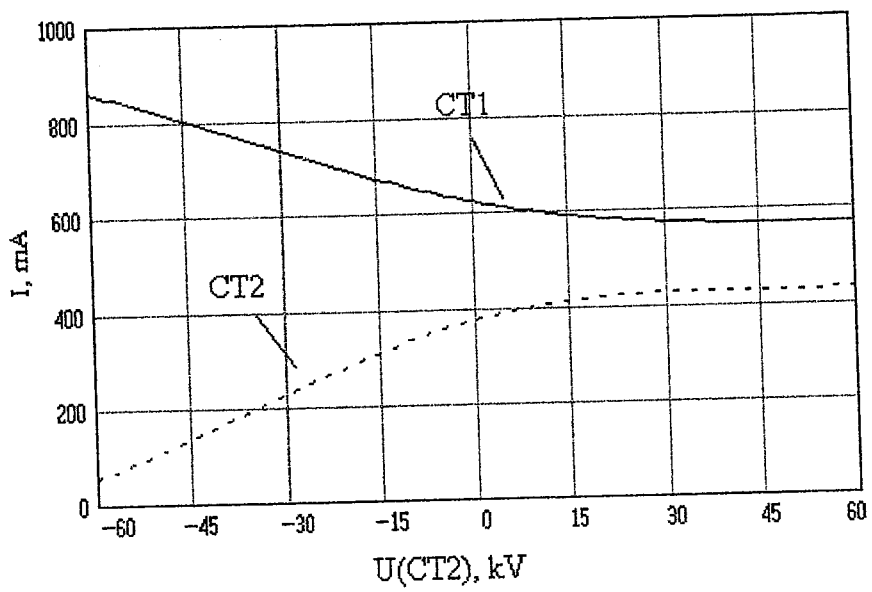

Fig.6. Current of the beam collection on CT1 (above) and CT2 + Window (below) versus potential of the CT2 for U(CT1)=60kV. Total beam current is 1A.

Total results for case if U(CT1)=75kV and U(CT2) is varied are shown on the Tab.3 and Fig.7. Details of beam dynamics in this case it can see in the Appendix I (Fig.28-Fig.32).

Table 3

U(CT2), kV	I(CT1), mA	I(CT2), mA	I(Window), mA	I(CT2)+I(Window), mA
-60	880	32	16	48
-40	807	99	67	166
0	595	102	298	400
40	531	140	319	459
60	530	138	322	460

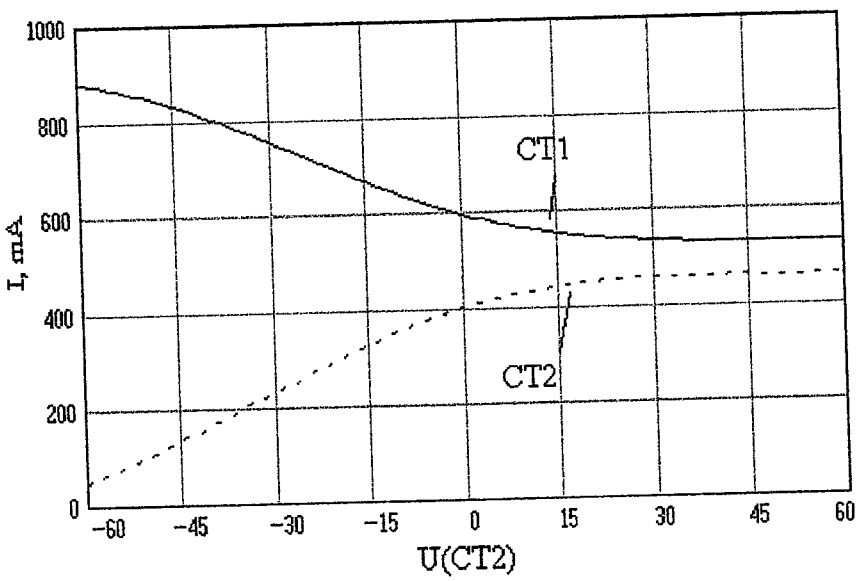

Fig.7. Current of the beam collection on CT1 (above) and CT2 + Window (below) versus potential of the CT2 for U(CT1)=75kV. Total beam current is 1A.

MAIN RESULTS OF PRIME BEAM DYNAMICS SIMULATIONS:

1. Change of the collector potential CT1 in the range 40-75kV does not influence the distribution of collected beam current on collectors CT1 and CT2 if the potential of CT2 is changed from -60kV up to 0. If the CT2 potential is changed from 0 to 60kV the distribution variation is still very weak.
2. Increase of the CT2 potential from 0 up to 60kV does nearly not influence the beam current collected on CT1 and on CT2. Then it is no reason to use potential U(CT2)<-60kV, because in this case almost all the beam current is lost to the walls of CT1. Therefore U(CT2) should be in the range -60kV<U(CT2)<0.
3. Testing for other initial beam density distribution versus radius has shown very weak influence on the results.
4. Correlation between the beam energy spread after the wiggler and at the exit of the decelerator is obtained for an uniform initial beam density distribution. By change of potential of the collector CT2 it is possible to determine the high-energy limit of the electron beam after exiting the wiggler. For U(CT1)=75kV and U(CT2)= -40kV beam electrons with E=1.40-1.42MeV can reach the window and walls of CT2. For U(CT1)=75kV and U(CT2)= -60kV we can obtain particles which impinged on the walls of the CT2 with E=1.42MeV only.
5. Maximum beam current collected is 993.5mA for U(CT1)=75kV, U(CT2)=0V.

2.2. SECONDARY ELECTRON EFFECTS

Secondary electrons result for elastic (backscattered electrons) and inelastic (secondary electrons) scattering of the primaries electrons from the collector walls. For determination of the initial secondary electron characteristics expressions and recommendations of [4] were used.

2.2.1. BACKSKATTERED ELECTRONS

- Backscatter coefficient in η the [4] is defined as:

$$\eta = \frac{n_{BSE}}{n_B} = \frac{i_{BSE}}{i_B}, \qquad (1)$$

where n_b is the number of beam electrons incident on the specimen (corresponding current is i_B);

n_{BSE} is the backscattered electrons (backscattered current is i_{BSE}).

Backscattered electrons respond to composition (atomic number or compositional constant), local specimen surface inclination (topographic or shape contrast), crystallography (electron channeling), and internal magnetic fields (magnetic contrast).

For beam energy range 4÷40keV coefficient η in the [4] is determined as

$$\eta(Z,E) = E^m C, \qquad (2)$$

where $m = 0.1382 - \frac{0.9211}{\sqrt{Z}}$;

$$C = 0.1904 - 0.2235(\ln Z) + 0.1292(\ln Z)^2 - 0.01491(\ln Z)^3 .$$

For copper of the collector :

Z=29

m= - 0.03284

C=0.3335

η(Z=29, E=4keV)=0.3187

η(Z=29, E=40keV)=0.2955

If to use these equations for all dispersion of energies which is of interest the following means for the backscatter coefficient may be received:

η(Z=29, E=0)=0.3335

η(Z=29, E=100keV)=0.2867

η(Z=29, E=140keV)=0.2835

It's a very weak dependence of η on the beam energy.

The backscatter coefficient depends on tilt angle θ (angle between the beam and the normal to the surface plane) [4]:

$$\hat{\eta}(\theta) = \frac{\eta(Z,E)}{(1+\cos\theta)^p}, \qquad (3)$$

where $p = 9/\sqrt{Z}$.

Results of some numerical estimates are written in the Tab.2:

Table 2.

θ°	0	10	20	30	45	60	75	90
$\hat{\eta}(\theta^\circ)$	0.3140	0.3180	0.3305	0.3525	0.4091	0.5078	0.6807	1

Angular distribution for backscattered electrons.

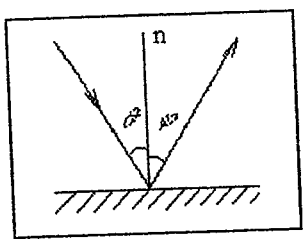

-For normal beam incidence (θ=0°) this distribution is follow [4]:

$$\eta(\varphi) = \eta_n \cos\varphi \qquad (4)$$

-Nonnormal beam incidence

Up to - cosine distribution may be used, for greater - angular distribution becomes progressively narrower parallel to the tilt axis. At very high tilt angles, e.g., the 80deg tilt case the distribution is sharply peaked in the forward direction, and relatively little scattering occurs parallel to the tilt axis [4].

Energy distribution

In corresponding to [4] $d\eta/dE$, where E=E(scattered)/E(beam), some beam energies are:

-For Cu and E(beam)=30keV $(d\eta/dE)max$ =0.18 if E(scattered)=0.9 * E(beam), i.e. E=0.9);

$d\eta/dE$=0.05..... E=0.5;

$d\eta/dE$=0.1..... E=(0.7, 1);

$d\eta/dE$=0.15..... E=0.8;

$d\eta/dE$=0.01..... E=0.2;

the coefficient $d\eta/dE$ is decrease with increase of the angle θ

$d\eta/dE$=0.18 if angle θ=0;

$d\eta/dE$=0.18.....θ=.22.5°;

$d\eta/dE$=0.15.....θ=45°;

$d\eta/dE$=0.08.....θ=67.5°.

In our model we used coefficient η=0.3 ÷ 1. for different angles according to Tab.2 as the total mean of the scattered beam, and energy E(scattered)=0.8 E (beam).

2.2.2. SECONDARY ELECTRONS

Total secondary coefficient δ is given by [4]:

$$\delta = \frac{n_{SE}}{n_B} = \frac{i_{SE}}{i_B}; \qquad (5)$$

- Energy distribution.

More then 90% have E<10eV [4].

δ≅0.1 for most elements (for beam energy Ebeam>10keV), dependence on atomic number of a target is absent [4].

Specimen Tilt Dependence [4]:

$$\delta(\vartheta) = \delta_0 \sec\vartheta \qquad (6)$$

2.2.3. INITIAL DATA FOR SIMULATIONS

Initial beam parameters for secondary effects were taken from results of prime beam dynamics simulations.

-In the region of the window (see Fig.1 and picture on this page).

Backscattered particles: $I_{II\,b} = 0.3I_I$ (as integral for all angles, all energies), $E_{II\,b} = 0.8E_I$, ray divergence after scattering is determined as $r' = \pi - \theta$ for each ray, where θ is the angle between prime ray and normal to surface. Here $I_{II\,b}$ is the current of backscattered beam, I_I - the prime beam current, $E_{II\,b}$ is the energy of the backscattered beam, E_I - energy of the prime beam.

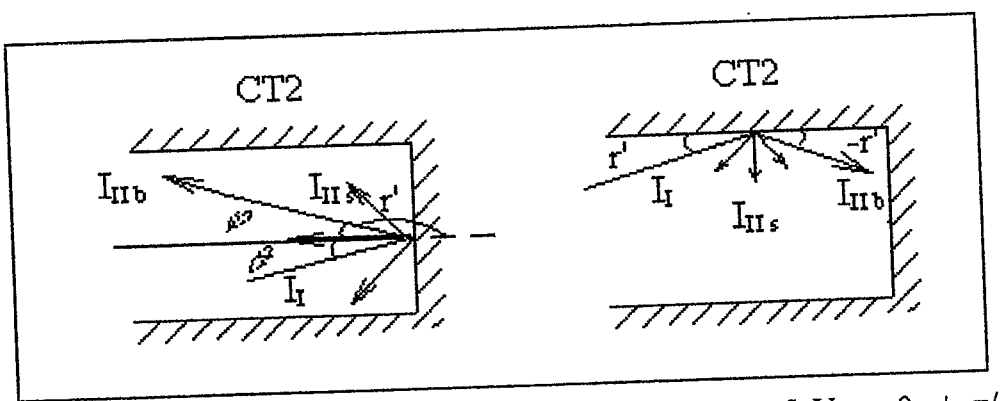

Secondary electrons: $I_{II\,s}=0.1I_I$, their energy: $E_{II\,s}$=5eV, φ=0, $\pm\,\pi/4$ with respect to normal of the window or $r'=\pi$, $\pm\,3\pi/4$ in the code EGUN [3] coordinate system.

Initial point of the backscattered and secondary electrons was determinate as final point for prime rays minus 1mm (because else this point can be out of the simulating region) after some iterations because backscattered and secondary electrons create a space charge which influence on the prime beam. In our case 4-5 iterations were used. My criterion was the difference between errors of simulations and relative change of results on the i - simulation with respect to i - 1.

- At the walls of the collector (see Fig.1 together with the picture on the page 15).

Backscattered particles: $I_{II\ b}=0.3I_I$, $E_{II\ b}=0.8E_I$, $r' = -\theta$, r =23.5mm (0.5mm smaller then radius of the collector tube because else this point can be out of the simulating region).

Secondary emission: $I_{II\ s}=0.1I_I$, $E_{II\ s}=5eV$, $r'= -\pi/2, -\pi/4, -3\pi/4$ in the code EGUN [3] coordinate system, r=23.5mm.

2.2.4. ANALYSIS OF SECONDARY ELECTRON EFFECTS

Our collector has a long region without a longitudinal gradient of the potentials. As a result secondary electrons can move perpendicular to the collector surface and they don't influence the longitudinal distribution of the collected beam. But secondary electrons have a space charge, which influence the prime electrons and backward streaming electrons. Secondary electron rays in the window region are shown on the Fig.8. The potential of the first tube of the collector U(CT1)=75kV will be used because its influence on the collection is very weak. Potential U(CT2)=0 in Fig. 8, but in this case it's not important for secondary electron motion. There are secondary electron rays from the walls only in the Fig.9. Initial velocity of these rays are perpendicular to the wall. Many electrons return to the initial positions due to opposite sign of the walls, there is little kinetic energy and an absence of potential gradients in any directions. All secondary electron rays are shown on the Fig.10. We can note the influence of space charge of electrons emitted from the window region on the secondary electrons which are emitted from the walls of the tubes. Motion of the secondary electrons with initial velocity emission angles of $r'=0$, and for $r'=\pm \pi/4$ in respect to surface are shown on the Fig. 11.

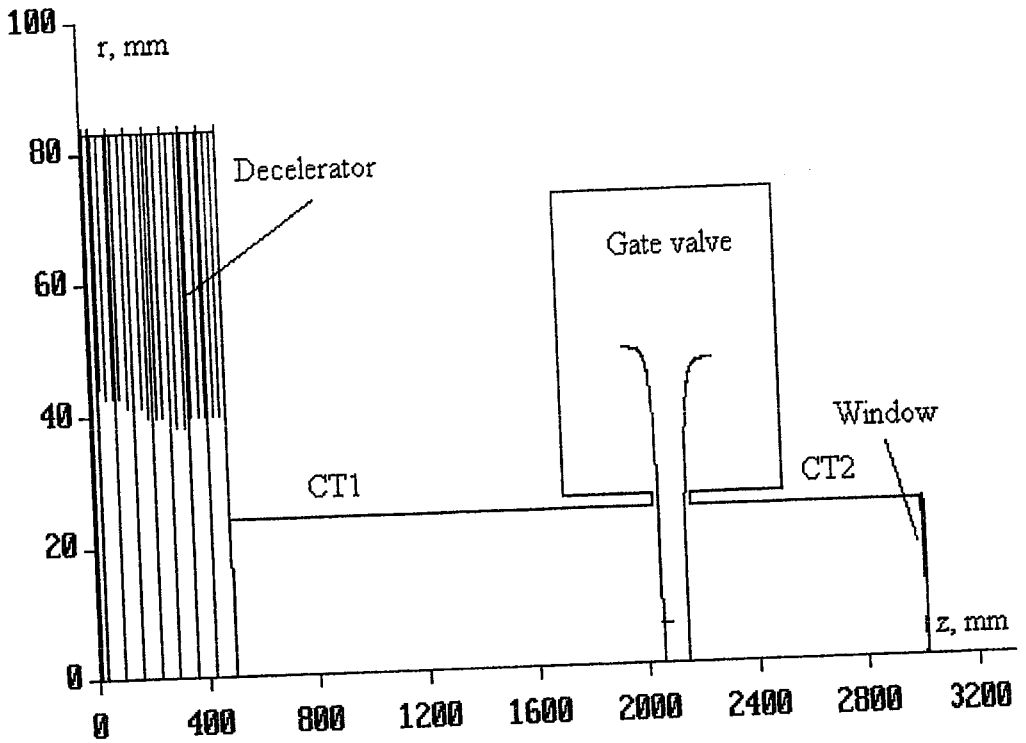

Fig.8. Secondary electron rays on the window region only.

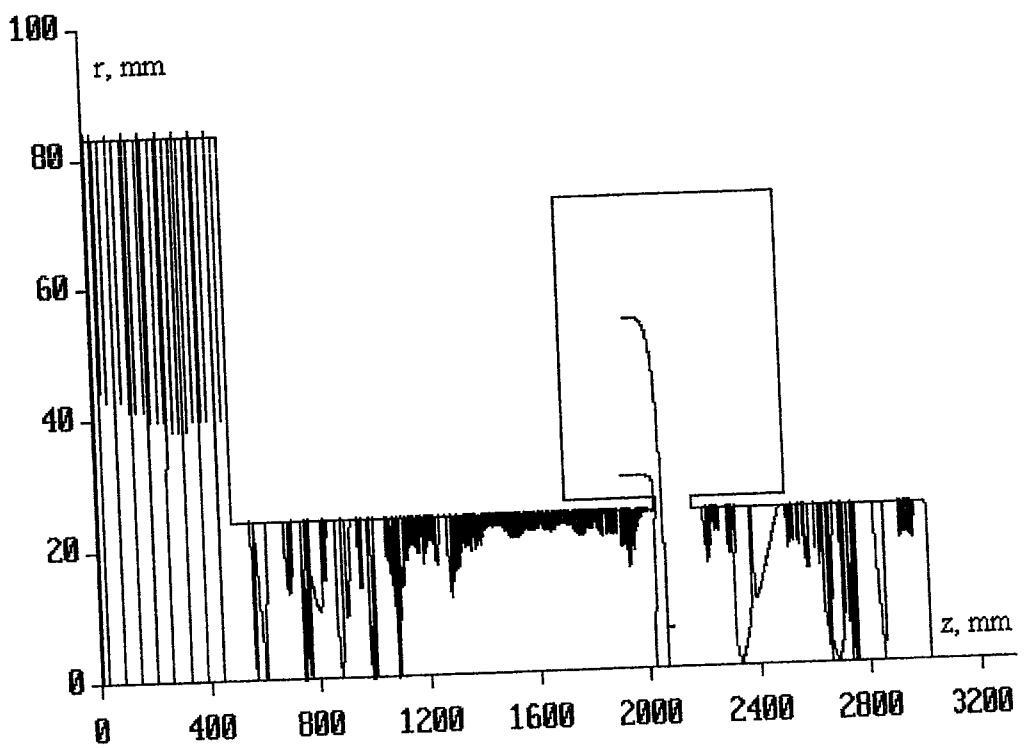

Fig.9. Secondary electron rays emitted from the walls only.

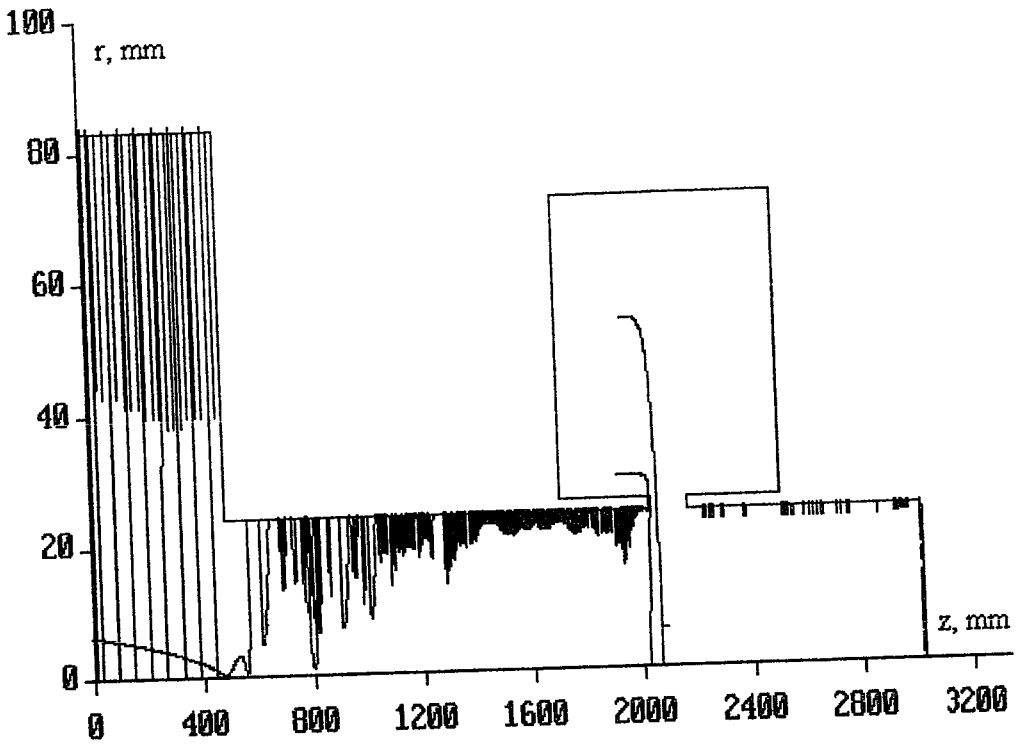

Fig.10. Secondary electron rays in the two-stage collector, which are emitted from walls and window region. Initial velocity is perpendicular to surfaces of the wall and the window.

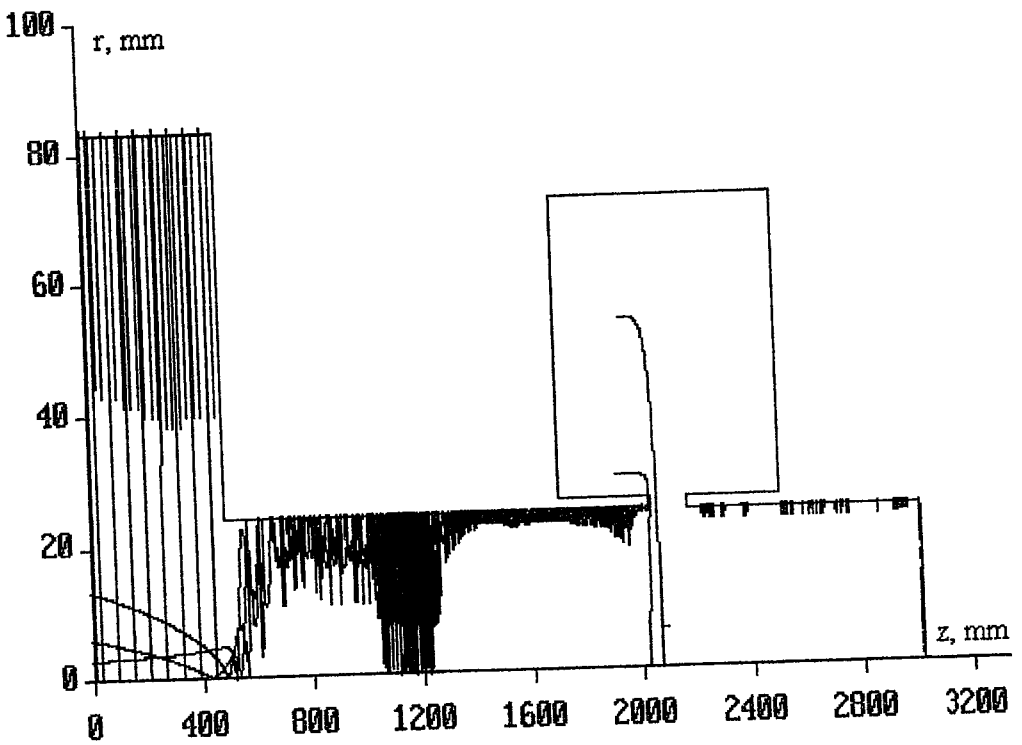

Fig.11. Secondary electron rays in the two-stage collector. Initial velocity angles r'=0, $\pm\pi/4$ in respect to surfaces of the wall and window.

Regarding situation with backskattered electrons. These electrons are the result of elastic scattering of beam electrons on the inside surface of the collector. Each backskattered electron ray of walls is described by one vector with the angle to surface $r'=-\theta$. Backskattered electron rays of the window region are described by one vector with angles $r' = \pi-\alpha$. On this region some backskattered electrons can attain the decelerator and to accelerate in the direction which is opposite to the prime beam. This process is very important but now we can know backward beam current only approximately because in order to obtain an accurate result it is necessary to determinate the dynamic aperture of the collector in opposite direction. But even for determination of beam rays tracing (primes, backwards) it's necessary to do some iterations (4÷5 for our case), because under action of the space charge of the secondary electrons final coordinates and angles, i.e. points on the phase space, are changes.

Results of beam dynamics simulations including prime, backscattered and secondary electron rays together are shown in the Appendix 2. It's possible to see that longitudinal prime beam distributions in this case differ essentially from prime beam distributions without secondary effects (see results on the Appendix 1). But accumulative results for each of the two stages of the collector is very little, it is illustrated by Fig. 12. There are curves for following cases described here: 1) if prime beam only was taken into account (curves 2,4 - the same as curves on the Fig.7.) and 2) prime beam moves in the fields of the secondary electrons (curves 1, 3). It's possible to see that this influence is weak.

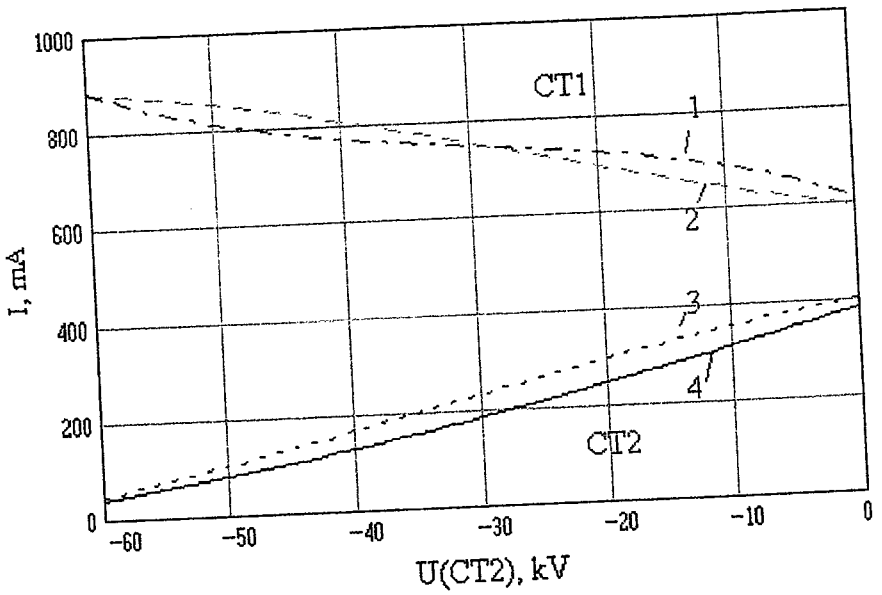

Fig.12. Current of the prime beam collections on CT1 and CT2 stages of the collector versus potential of the CT2 for U(CT1)=75kV.

3. METHOD OF CURRENT MEASUREMENTS ON CT1, CT2

Results of longitudinal collected beam distribution for cases of prime beam only and prime beam together with secondary electron effects are described above. But we can't measure currents of each beam ray. We can measure current output from the collector but which carry information about the beam. The scheme of measurements which is proposed for realization can be seen in the Fig. 13. Voltages of the U1 and U2 determine the potential of the collector stages, and their common point is under potential of the electron gun cathode (-43kV relative to ground). Current directions on Fig.13 corresponds to direction of the beam.

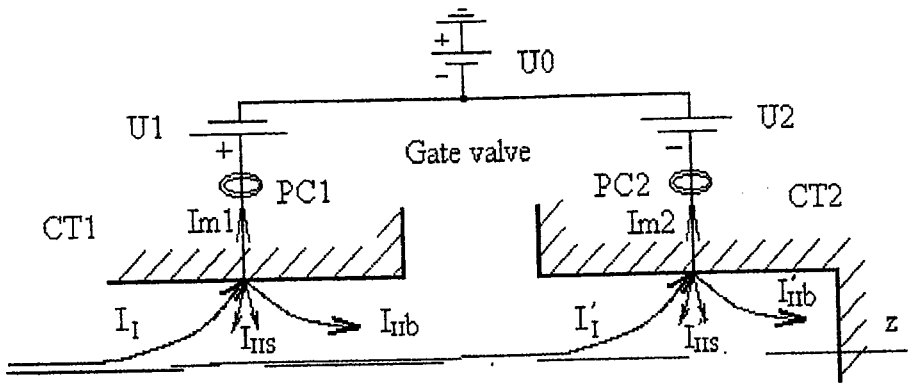

Fig.13. Scheme of collecting current measurements. U1,U2 - voltage sources of the collector, U0 - voltage source of the electron gun; PC1, PC2 - Pearson coils; Im1, Im2 - measured currents.

The measured total currents Im1 and Im2 for the two stages of the collector determined as:

$$I_{m1,m2} = \sum_i \left[\left(I_{1i} - I_{11bi} - I_{11si} \right) + \sum_k \left(I_{11bki} + I_{11ski} \right) \right]; \qquad (8)$$

where I_{1i} - i-th ray prime beam current;

I_{11bi} - backscattered beam current, delivered by i-th ray of the prime beam;

I_{11si} - current of secondary electrons, delivered by i-th ray of the prime beam;

I_{11bki} - backscattered beam current, which enters into i-point from other, k-point;

I_{11ski} - current of the secondary electrons, which enters into i-point from other, k-point.

Our two-stage collector have long regions with uniform electric potentials. Secondary emission electrons with their little kinetic energy, which move in this field,

or return to the wall (from which started or attain up to opposite wall). But we work with axial-symmetry structure, on which these two possibilities are equivalent and we don't take into account secondary electron currents I_{11si} and I_{11sk}. A relatively short regions with longitudinal gradient of the potential on the ends of each potential tubes CT1 and CT2 carry a perturbation on beam dynamics not more then error of simulations (some percents). For other collector geometry, contribution of the secondary electrons into measured collected currents may be visible.

The simulated currents, which can be measured in corresponding to Fig.13 scheme, for U(CT1)=75kV as a function of the U(CT2) are shown on the Fig.14. With increasing of the negative potential U(CT2) beam losses increase in the gate valve region and backward current increase. It is the reason of the slow changes of the Im1 for above values of U(CT2).

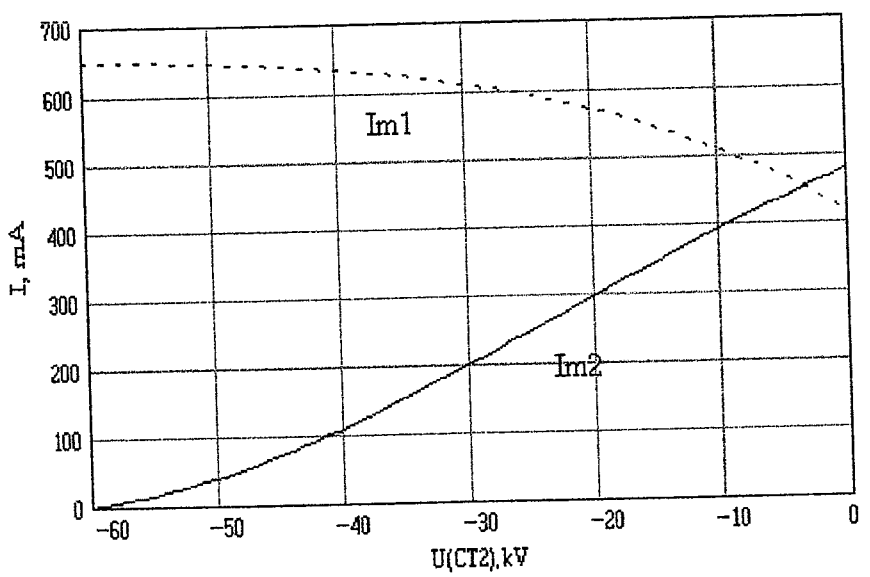

Fig.14. The currents on CT1 and CT2 stages of the collector in the points of current measurements versus potential of the CT2 for U(CT1)=75kV. Currents are determined by prime and backscattered beams.

To determinate the power which is collected in the collector we can write the follow expression:

$$P_{m1.m2} = f\sum_i \left[E_{1i}\left(I_{1i} - 0.8I_{11bi}\right)\right], \quad (9)$$

where f - duty factor;

E_{1i} - beam energy for i-th prime ray, eV.

On this approximation backward beam is absorbed by walls of the collector completely. Results of the simulations for f=1 (i.e. peak means) are shown on the Fig.15.

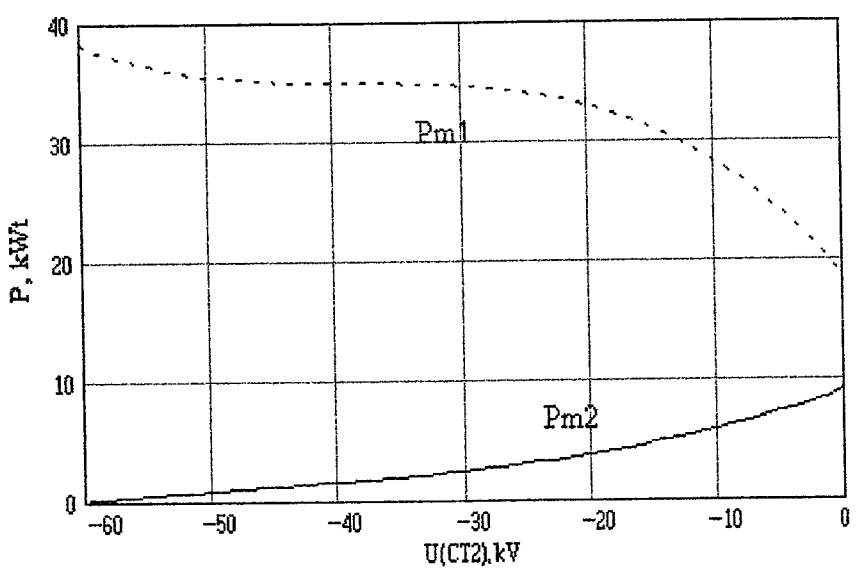

Fig.15. The simulated power dispersed on CT1 and CT2 stages of the collector versus potential of the CT2 for U(CT1)=75kV.

Results of simulations for multiple beam scattering on the collector are shown below. For these simulations expressions (8) and (9) were used with changing of indexes correspondingly.

MULTIPLE BEAM SCATTERED EFFECTS AND EFFICIENCY OF THE TWO STAGE FEL COLLECTOR

Efficiency of a collector is determined as ratio of collected beam current on the collector to total prime beam current on the collector enter (1A in our case). For calculations of the collector efficiency effects of frequent beam elastic scattering on the collector walls were taken into account. Expressions (8) and (9) were used recurrently, i.e. secondary beam after its first scattering was used as initial beam for second scattered action and so on. Simulations were continued up to the situation in which the current difference between successive iteration is commensurable to the accuracy of simulations. From 5 to 6 scattering were simulated. Correspondingly means of simulated current which will be measured and its power dispersion were changed slightly (see Fig. 14 and Fig. 15) and these results are shown on the Fig. 16 and Fig.17.

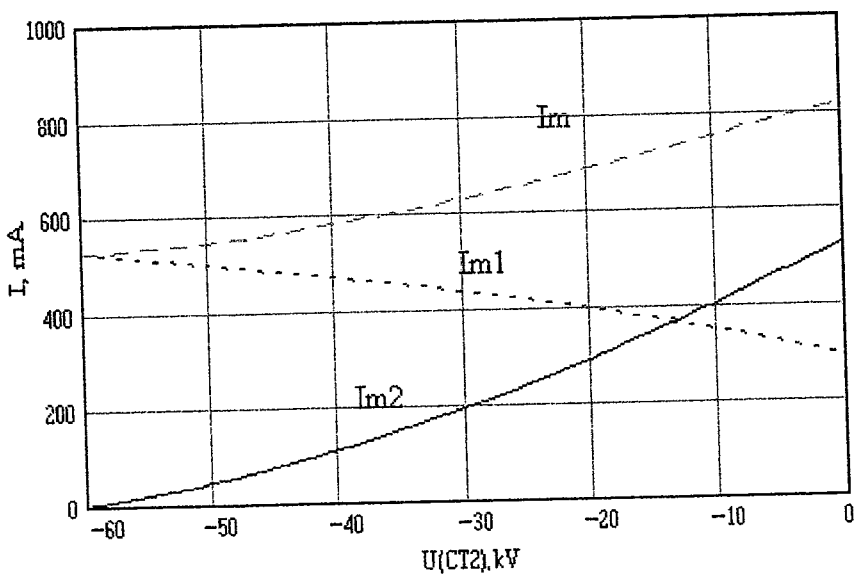

Fig.16. The collected currents Im1, Im2 in CT1, CT2 stages of the collector in the current supplied points versus U(CT2) correspondingly and their sum Im for U(CT1)=75kV. Multiple beam scattering.

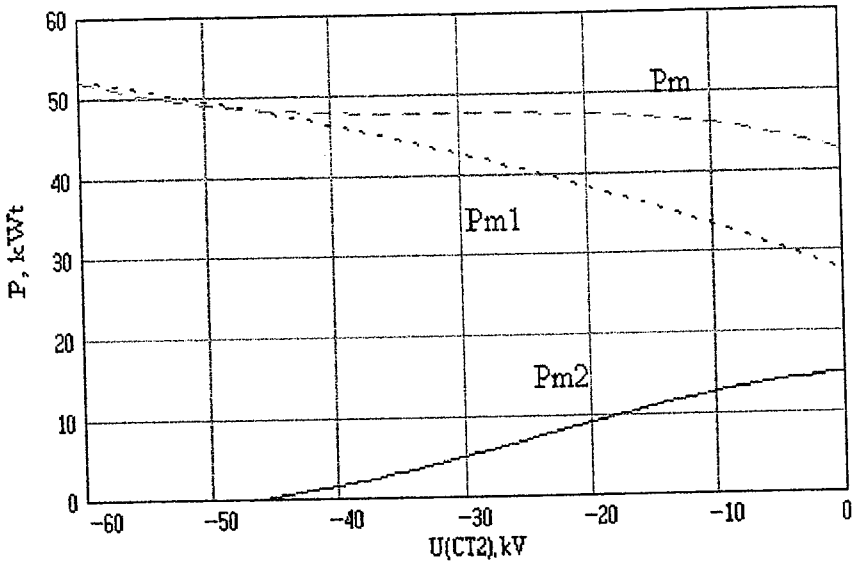

Fig.17. The collected power dispersion Pm1, Pm2 on CT1, CT2 stages of the collector correspondingly and their sum Pm versus potential U(CT2) for U(CT1)=75kV. Multiple beam scattering.

Two stage collector efficiencies δ for some potentials of the second stage U(CT2) are shown on the Table 3. Results are writen for two cases: if prime and secondary effects were taken into account (one act of scatter); if high order effects were taken into account (multitude beam scattering).

Table 3.

Two stage collector efficiencies δ for some potentials of the second stage U(CT2)

U2, kV	0	-20	-40	-60
δ, % one scattering	93.5	89.0	88.0	83.5
δ, % multiple scattering	82.9	72.0	69.6	66.3

CONCLUSION

The main characteristics of the two stage collector for Israeli FEL were determined using the computer code EGUN-2 [3] and information from ref. [4] for initial secondary electron effects data.

It is interesting to compare results obtained using prime beam dynamics simulations only with those obtained using secondary emission effects. The results of collecting current on the two of collector stages for a prime beam only and for a prime beam with secondary emission are taken into account are similar (Fig. 12), although the collected beam distributions differ much for these two cases. This difference may be seen by comparing figures for prime beam and prime beam plus secondary emission beam dynamics for U(CT1)=75kV and for various U(CT2) voltages; see appendixes: Fig. 30 compared with Fig. 33 (U(CT2)=0); Fig. 29 with Fig. 35 (U(CT2)= -40kV) and Fig. 28 with Fig.36 (U(CT2)= -60kV). A most interesting situation takes place for backscattered electrons which enter the decelerator and which accelerate in the opposite direction - towards the prime beam. With increasing negative potential U(CT2) the number of backscattered electrons from the window region decreases and for U(CT2)<-60kV it is equal to 0. But the number of backscattered electrons from the CT2 walls increase. The reason for this is that prime electrons invert direction and thus the back scattered electrons move to the decelerator. This effect determines the main problem for this design - the problem of the backward current, i.e. problem of the collector efficiency. Unfortunately to build a complete model simulating the beam dynamics for this case is very difficult. Initial beam parameters for secondary particle emission were taken approximately.

For calculations of the collector efficiency, effects of frequent beam elastic scattering on the collector walls were simulated. Counting of these high order effects

decrease calculated coefficient of the collector efficiently δ. So, it is changed from 93.5% for case only secondary effects simulations to 83% for high order effects for U(CT2)=0; from 83.5% to 66.3% for U(CT2)=-60kV. In such a manner, efficiency of the two stage collector is not good enough and high order scattering are visible. But it is characterized by long regions with continuous potentials, that creates the possibility of ignoring secondary electrons as result of inelastic scattering.

In the near future experiments with this collector design are planned. Additional information is required for beam dynamics simulations, particularly for simulation and design of the multistage collector for our FEL. Our present simulation did not take into account the influence of collector potentials on intensity of secondary electron emission. The contributions of secondary electrons on the collected current was assumed to be negligible, but for some geometries this effect may be considerable.

In this work follow specialists participated: Prof. A.Gover - main idea, heading of the work; J.Sokolowsky, M.Canter - construction of the collector and experimental part of the work; G.Wolowelsky - technical design; A.Abramovich, Y.Pinhasi - data for initial beam parameters, A.Eichenbaum, H.Kleinman, M.Tecimer, A.Yahalom - fruitful discussions.

REFERENCES

1. A.Abramovich et al., "Investigation and simulation of the electron energy spread after interaction region on the ISRAELI tandem FEL", FEL-98 International Conference, Williamsburg, Phys. Rev. Lett. 82(26), 1999.

2. A.Abramovich, et.al., "Lasing and radiation-mode dynamics in a Van de Graaff accelerator-free electron laser with an internal cavity", Appl.Phys.Lett. 71(26), 1997.

3. W.B.Herrmannsfeld, "EGUN - an electron optics and gun design program", SLAC-Report-331, 1988 & lists with comments for new version, 1995.

4. J.T.Goldstein at al., "Scanning electron microscopy and x-ray microanalysis", Plenum Press, 1994.

APPENDIX 1. PRIME BEAM ONLY

Pictures of this appendix (Fig.18-Fig.32) illustrate prime beam tracing and longitudinal distributions of the collection beam in the two-stage collector region for various potentials of its two stages CT1 and CT2.

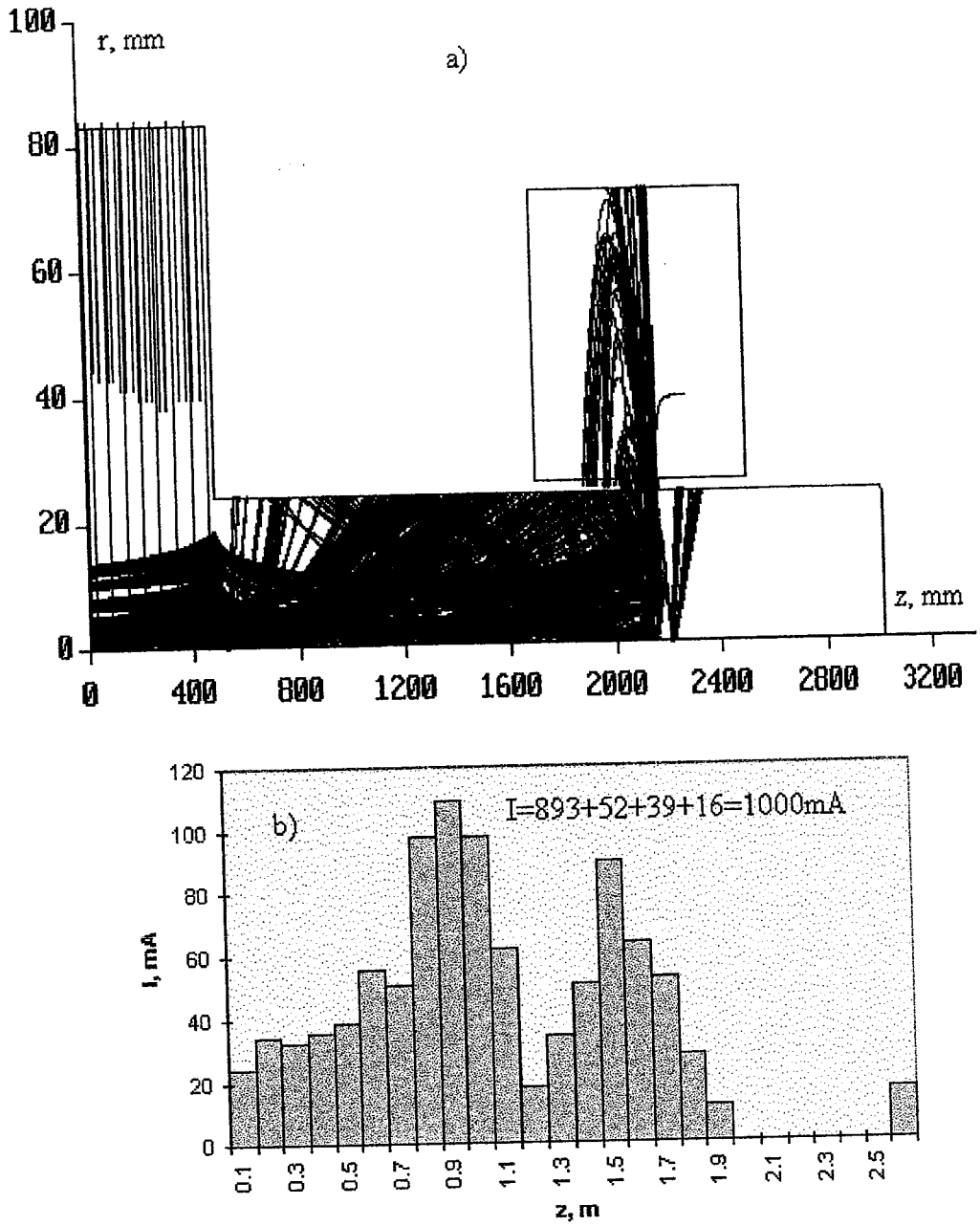

Fig.18. Trajectories of the rays in the region of the collector (a) and histogram (b) of the beam collection in longitudinal direction with step Δz=0.1m for U(CT1)=40kV, U(CT2)= -60kV.

There are two parts of the collector: CT1 - the new tube from 10^{th} electrode of the decelerator (z=0.1m on the histogram) up to the gate valve (z=1.7m) and the CT2 - old tube after prolongation (z=1.8-2.7m). Above on the histogram - beam

collection in the parts of this construction: 893mA - in the CT1, 52mA - in the gate valve, 39mA - in the CT2, and 16mA - in the window. Potentials are denoted respectly with ground (the anode of the electron gun). Potential of the electron gun cathode is -43kV. The returned beam current, which enters in the decelerator in opposite direction, is not more then 2mA for any looking through collector potentials.

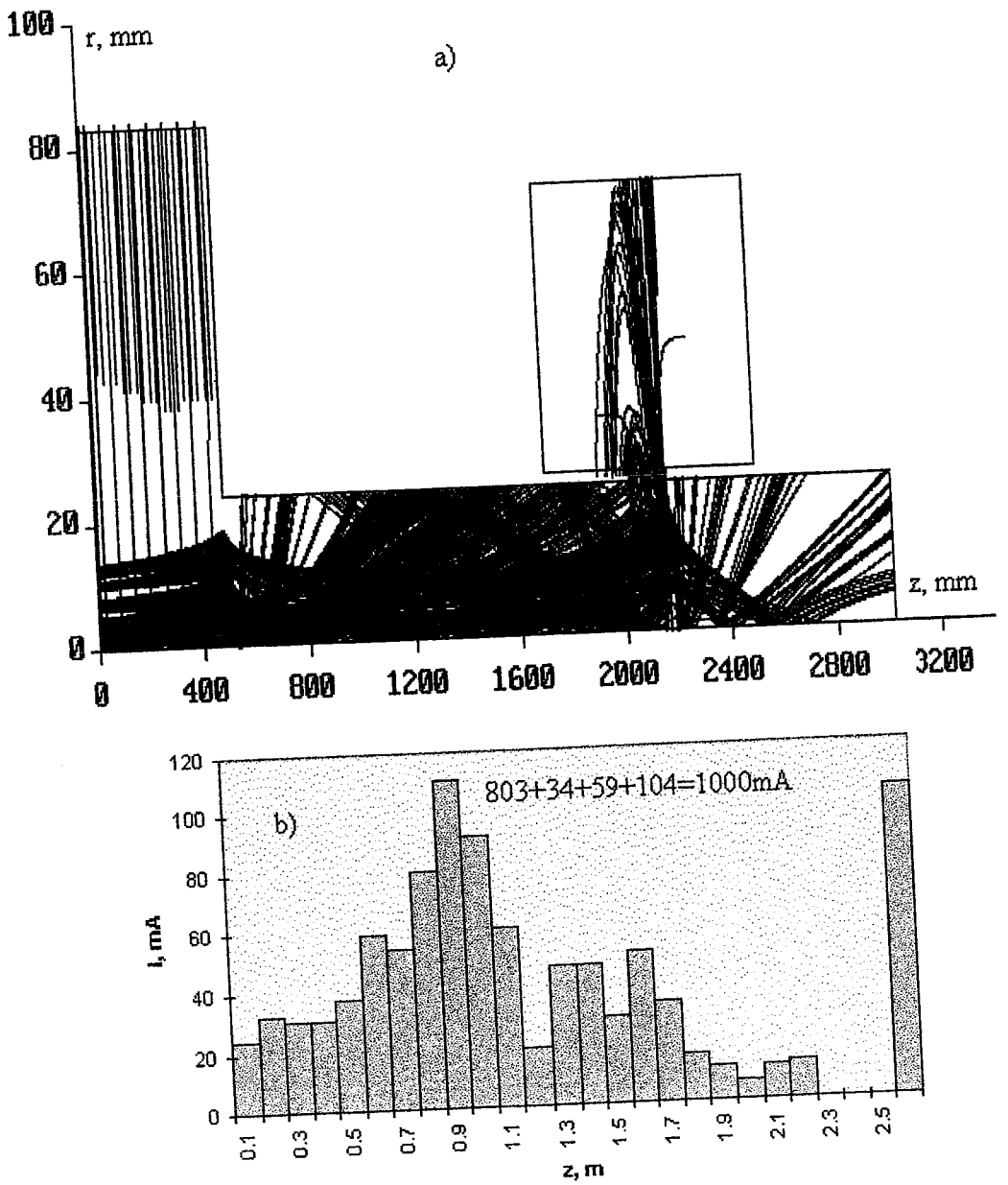

Fig.19. Trajectories of the rays in the region of the collector (a) and histogram (b) of the beam for U(CT1)=40kV, U(CT2)= -40kV.

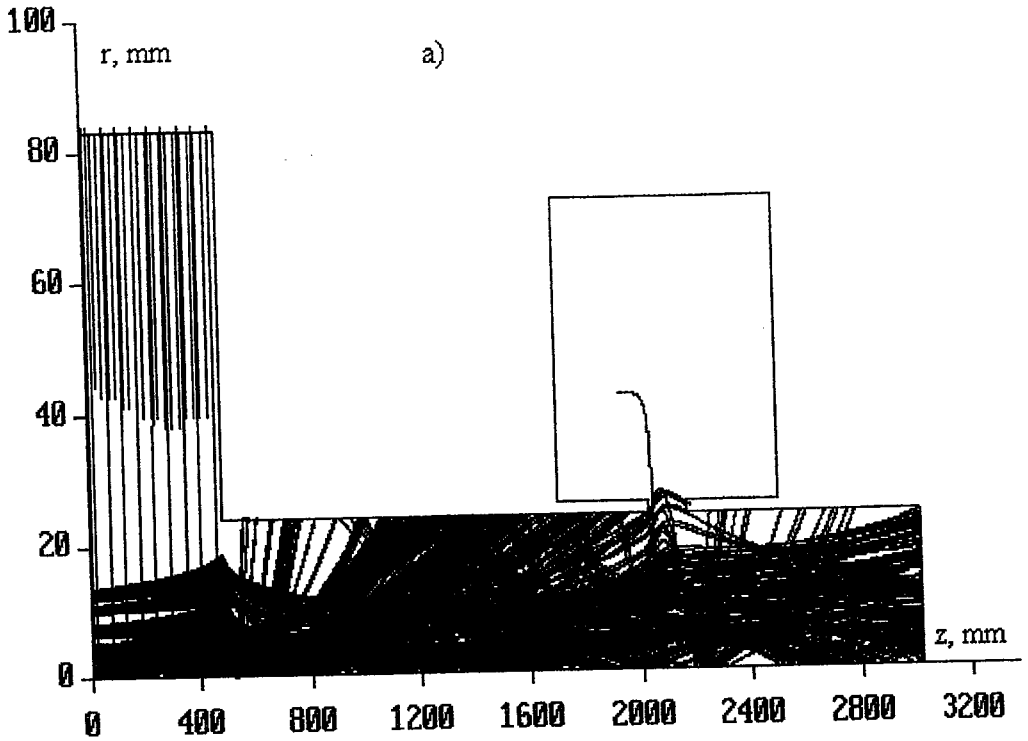

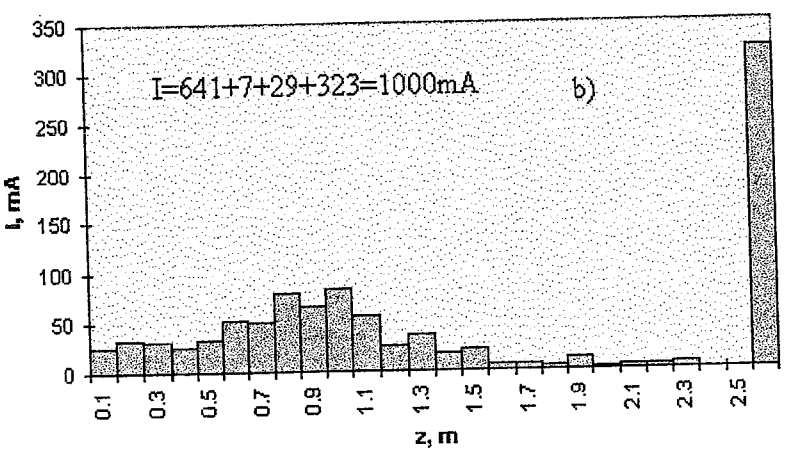

Fig.20. Trajectories of the rays in the region of the collector (a) and histogram (b) of the beam for U(CT1)=40kV, U(CT2)= 0.

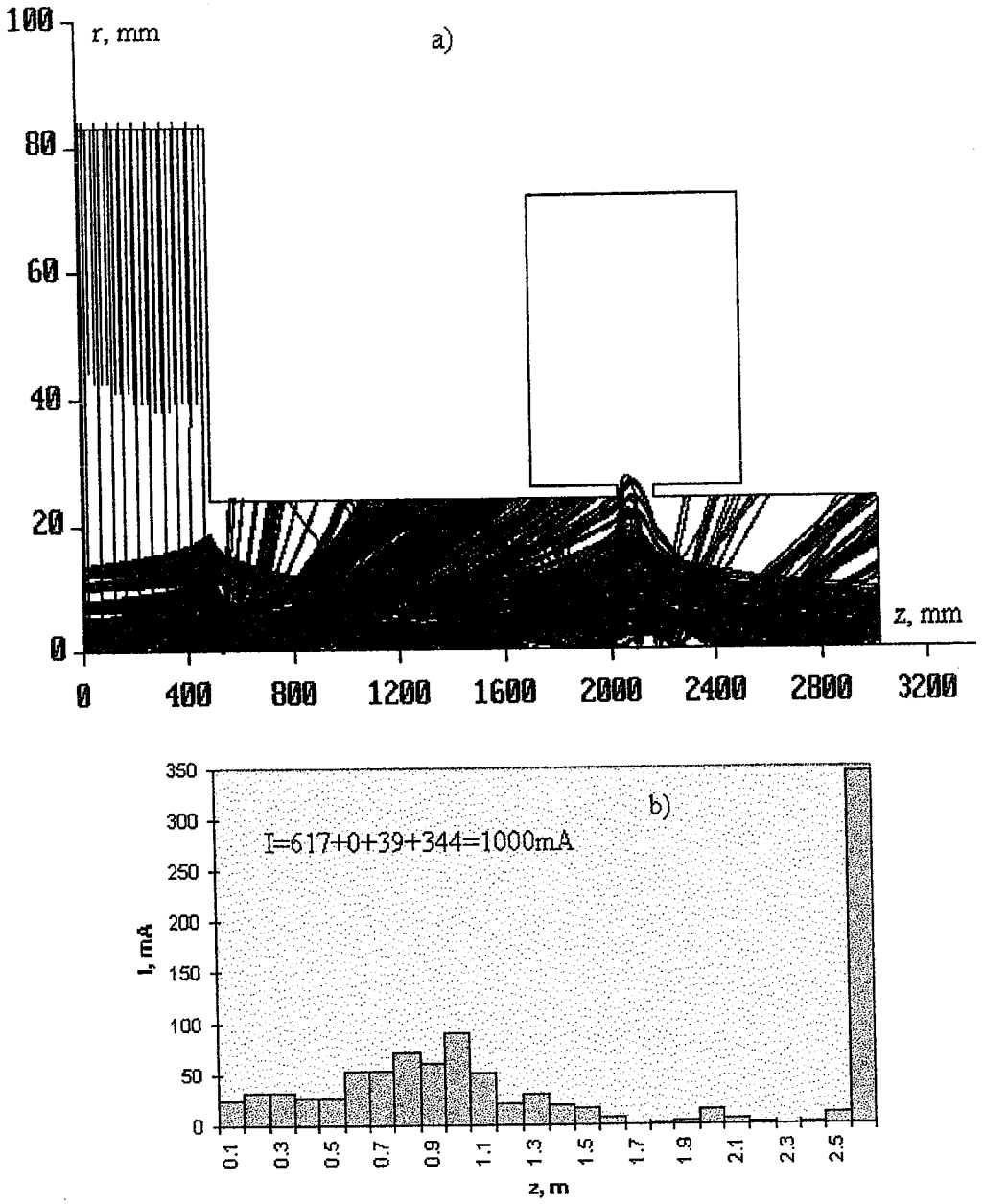

Fig.21. Trajectories of the rays in the region of the collector (a) and histogram (b) of the beam for U(CT1)=40kV, U(CT2)= 40kV.

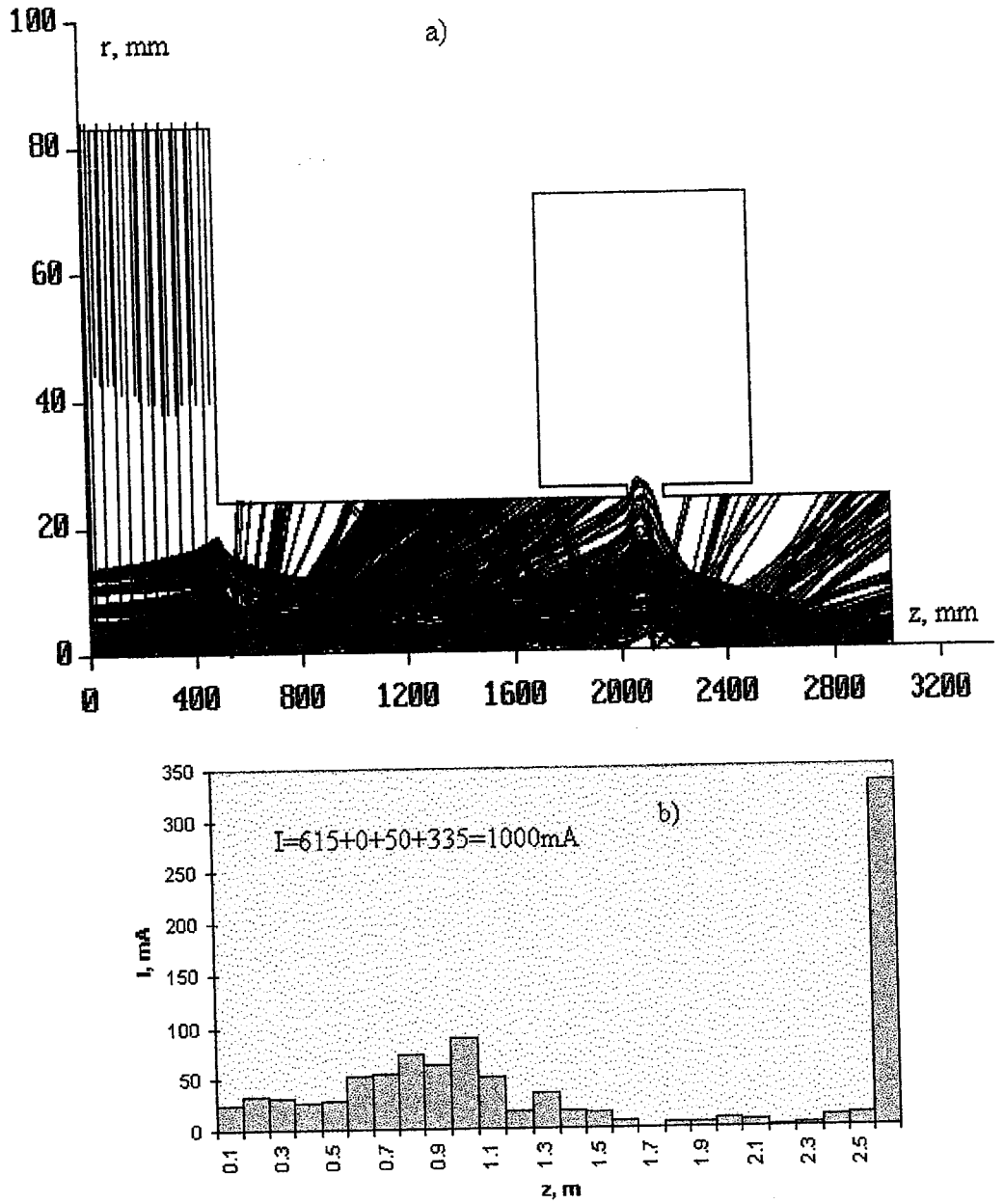

Fig.22. Trajectories of the rays in the region of the collector (a) and histogram (b) of the beam for U(CT1)=40kV, U(CT2)= 60kV.

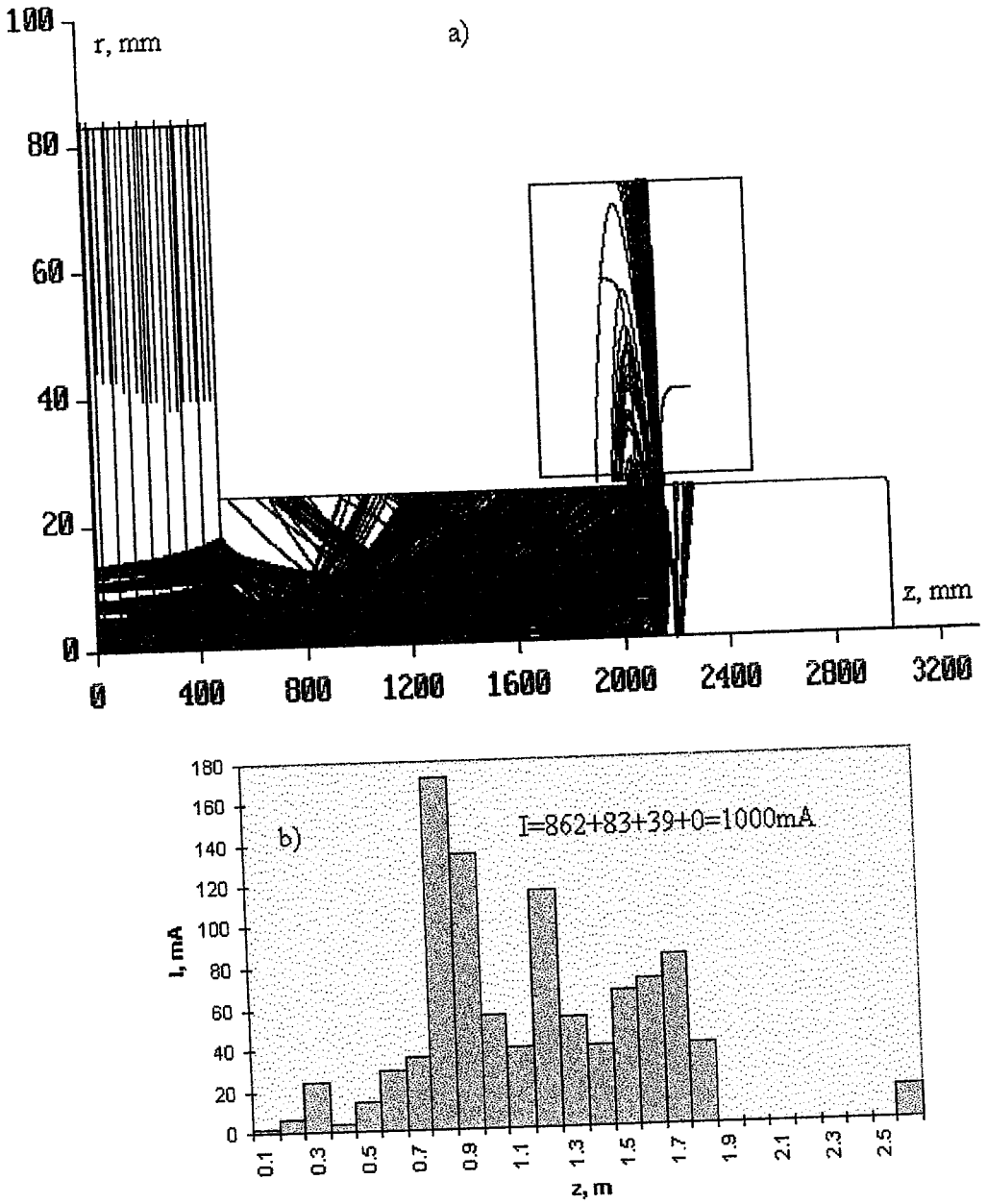

Fig.23. Trajectories of the rays in the region of the collector (a) and histogram (b) of the beam for U(CT1)=60kV, U(CT2)= -60kV.

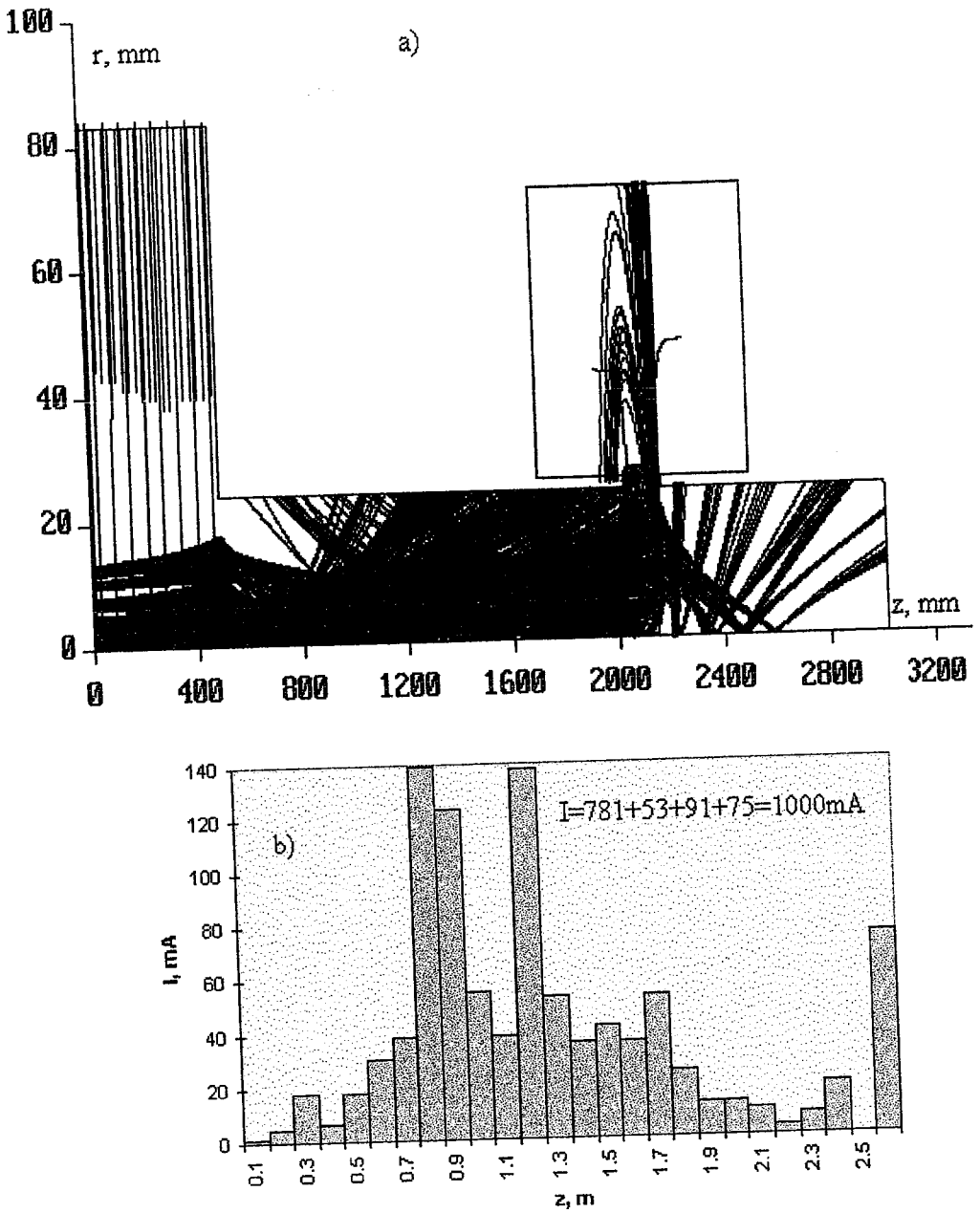

Fig.24. Trajectories of the rays in the region of the collector (a) and histogram (b) of the beam for U(CT1)=60kV, U(CT2)= -40kV.

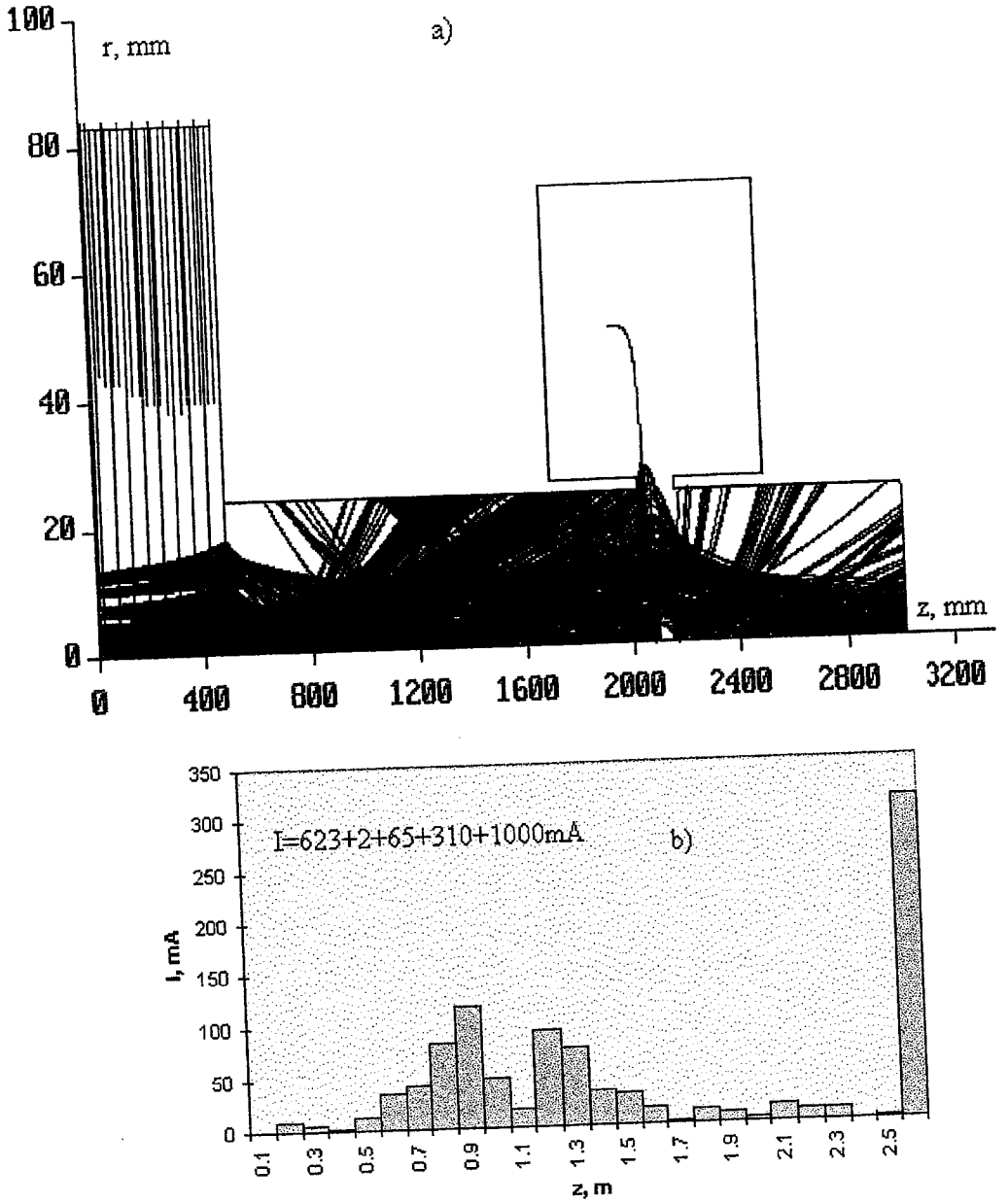

Fig.25.Trajectories of the rays in the region of the collector (a) and histogram (b) of the beam for U(CT1)=60kV, U(CT2)= 0.

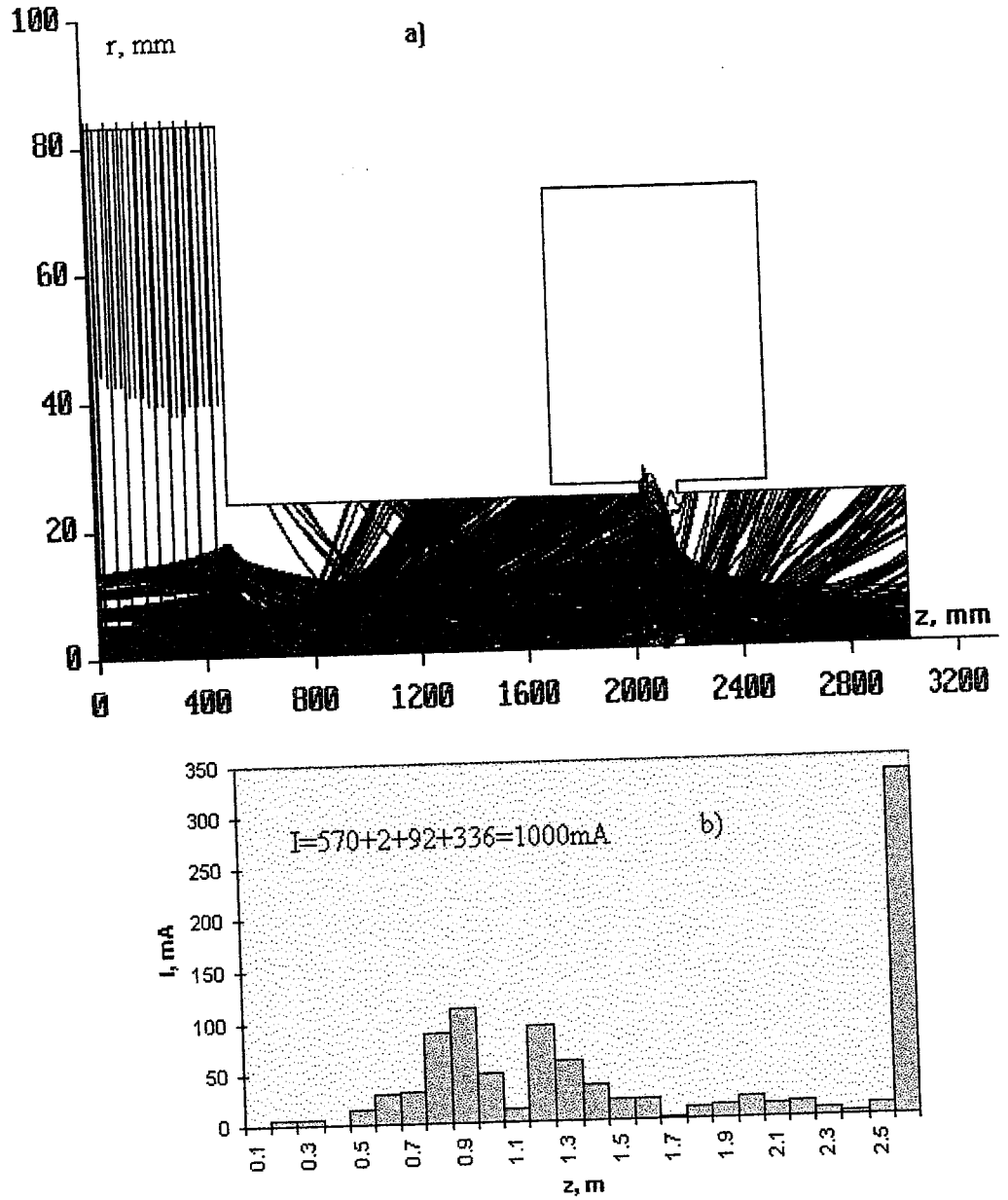

Fig.26 Trajectories of the rays in the region of the collector (a) and histogram (b) of the beam for U(CT1)=60kV, U(CT2)= 40kV.

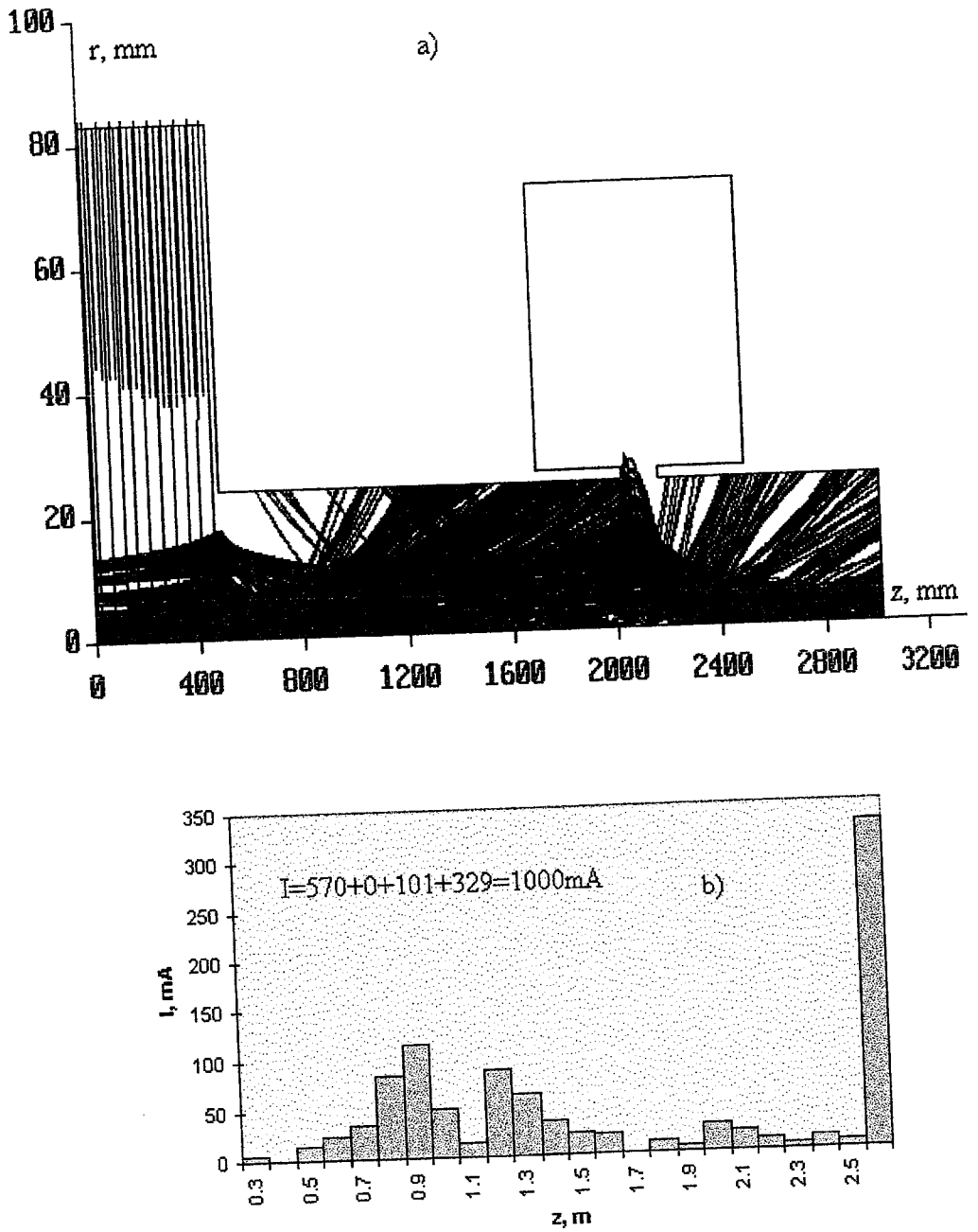

Fig.27 Trajectories of the rays in the region of the collector (a) and histogram (b) of the beam for U(CT1)=60kV, U(CT2)= 60kV.

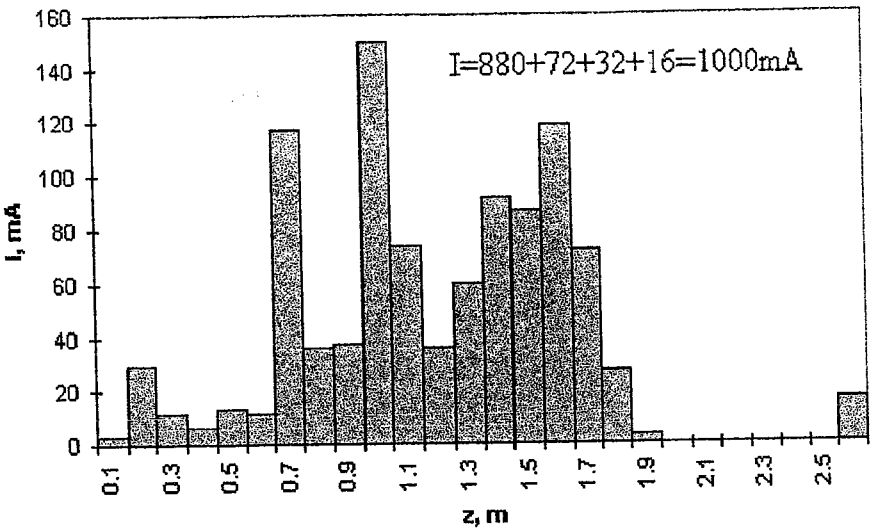

Fig.28. Histogram of the beam for U(CT1)=75kV, U(CT2)= -60kV.

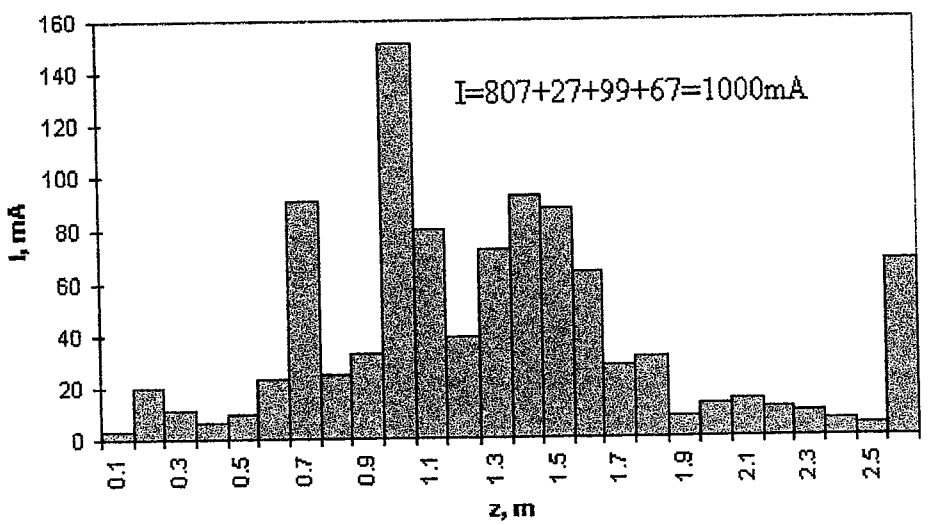

Fig.29. Histogram of the beam for U(CT1)=75kV, U(CT2)= -40kV.

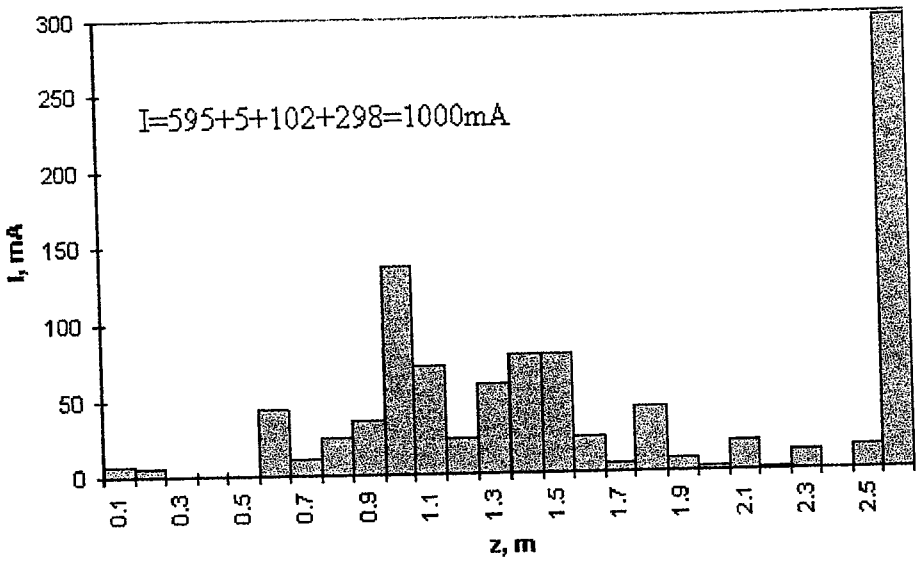

Fig.30. Histogram of the beam for U(CT1)=75kV, U(CT2)= 0.

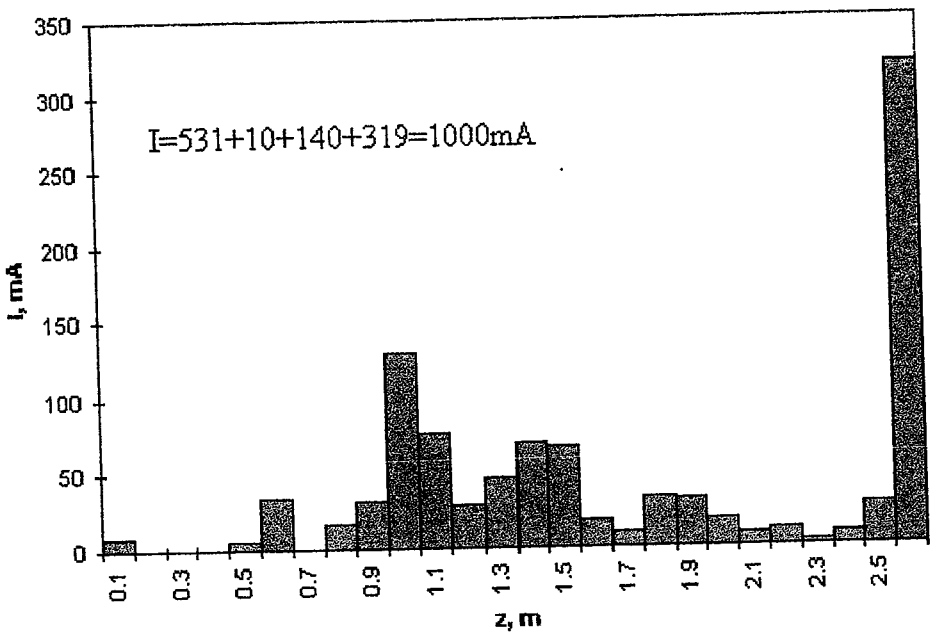

Fig.31. Histogram of the beam for U(CT1)=75kV, U(CT2)= 40kV.

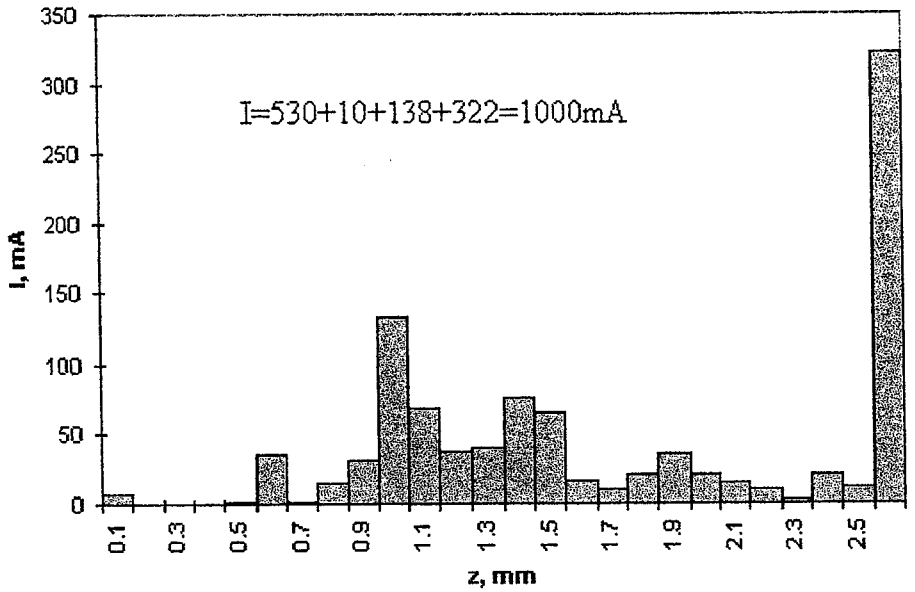

Fig.32. Histogram of the beam for U(CT1)=75kV, U(CT2)= 60kV.

APPENDIX 2. PRIME AND SECONDARY BEAM DYNAMICS

Pictures of this appendix (Fig.33-Fig.36) illustrate prime and secondary beam tracing in the two-stage collector region, longitudinal distributions of the collection as well prime as secondary beam for various potentials of the stage CT2.

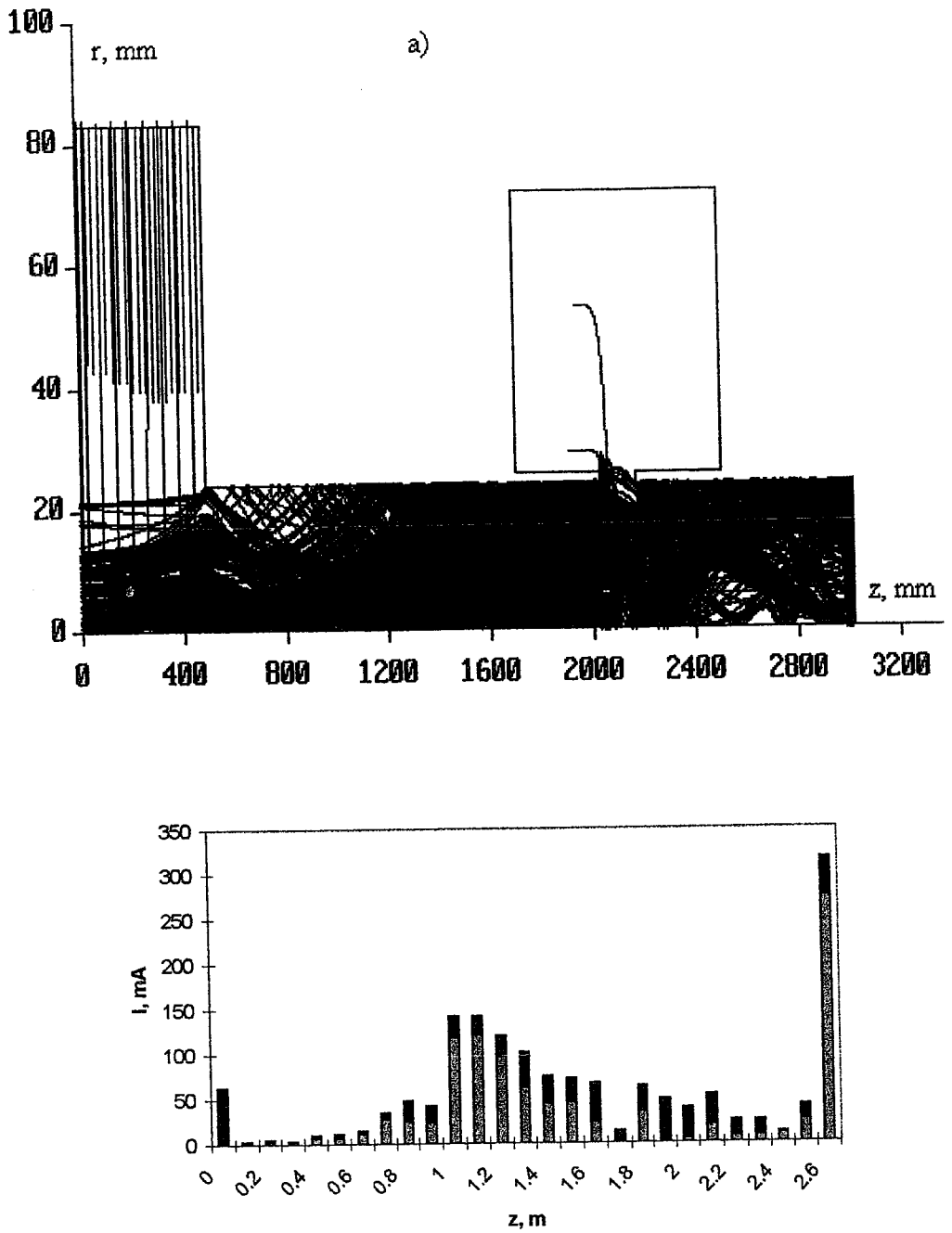

Fig.33. Beam ray trajectories (a) and histogram for prime (lower part of the each column) and backscattered (upper part) beam longitudinal distribution for U(CT1)=75kV, U(CT2)=0. Left column (position z=0) is the beam current which moves into the decelerator in opposite direction.

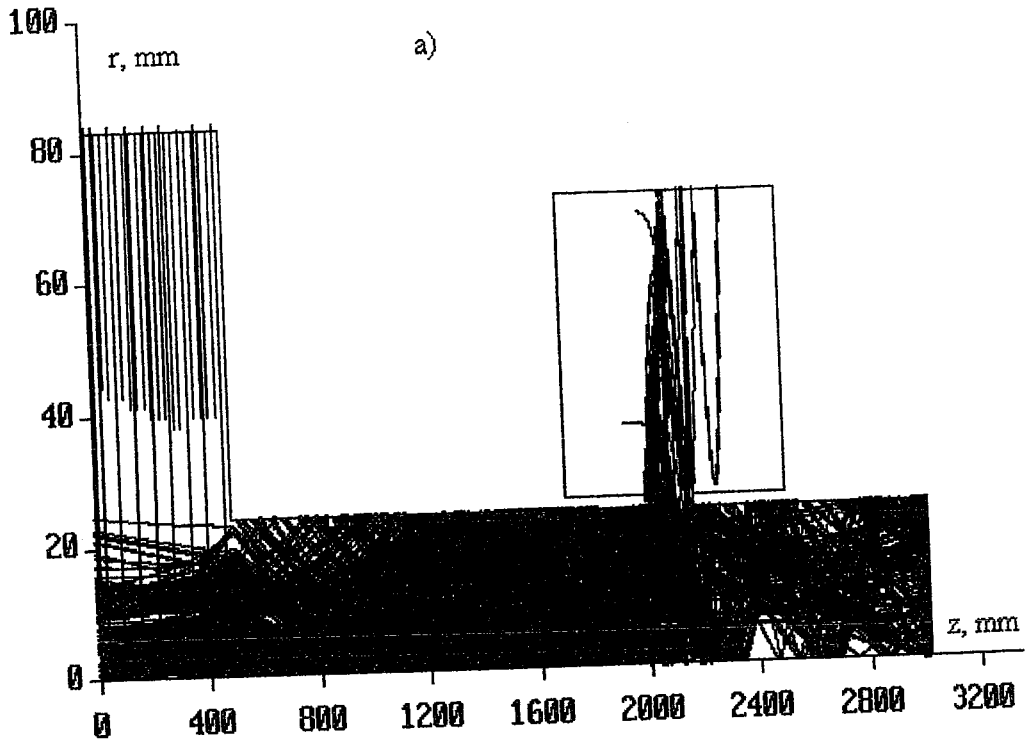

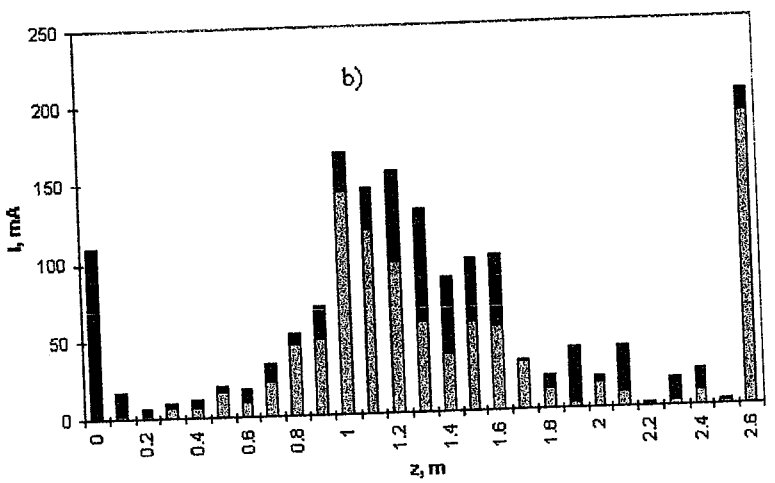

Fig.34. Beam ray trajectories (a) and histogram for prime (lower part of the each column) and backscattered (upper part) beam longitudinal distribution for U(CT1)=75kV, U(CT2)=-20kV. Left column (position z=0) is the beam current which moves into the decelerator in opposite direction.

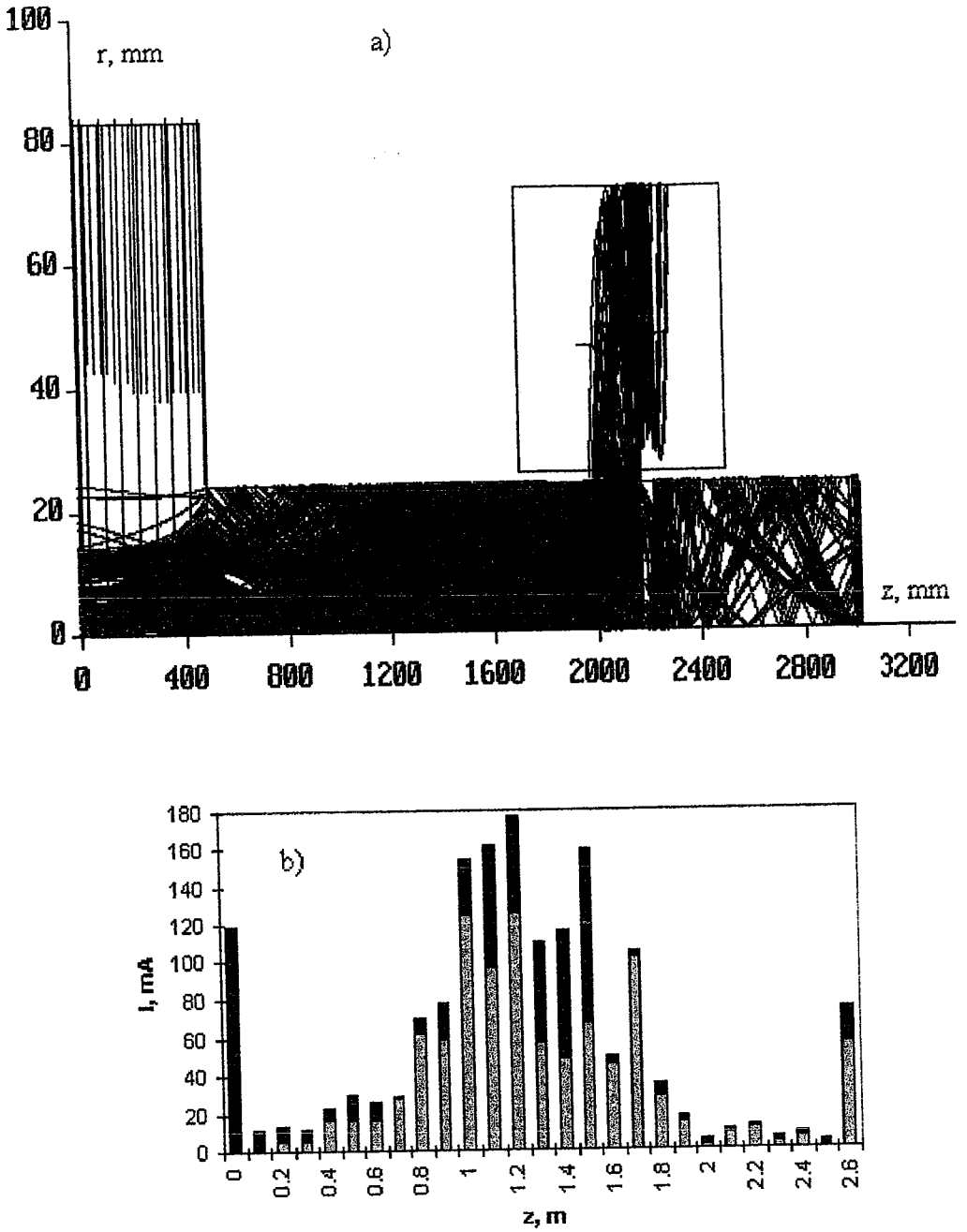

Fig.35. Beam ray trajectories (a) and histogram for prime (lower part of the each column) and backscattered (upper part) beam longitudinal distribution for U(CT1)=75kV, U(CT2)=-40kV. Left column (position z=0) is the beam current which moves into the decelerator in opposite direction.

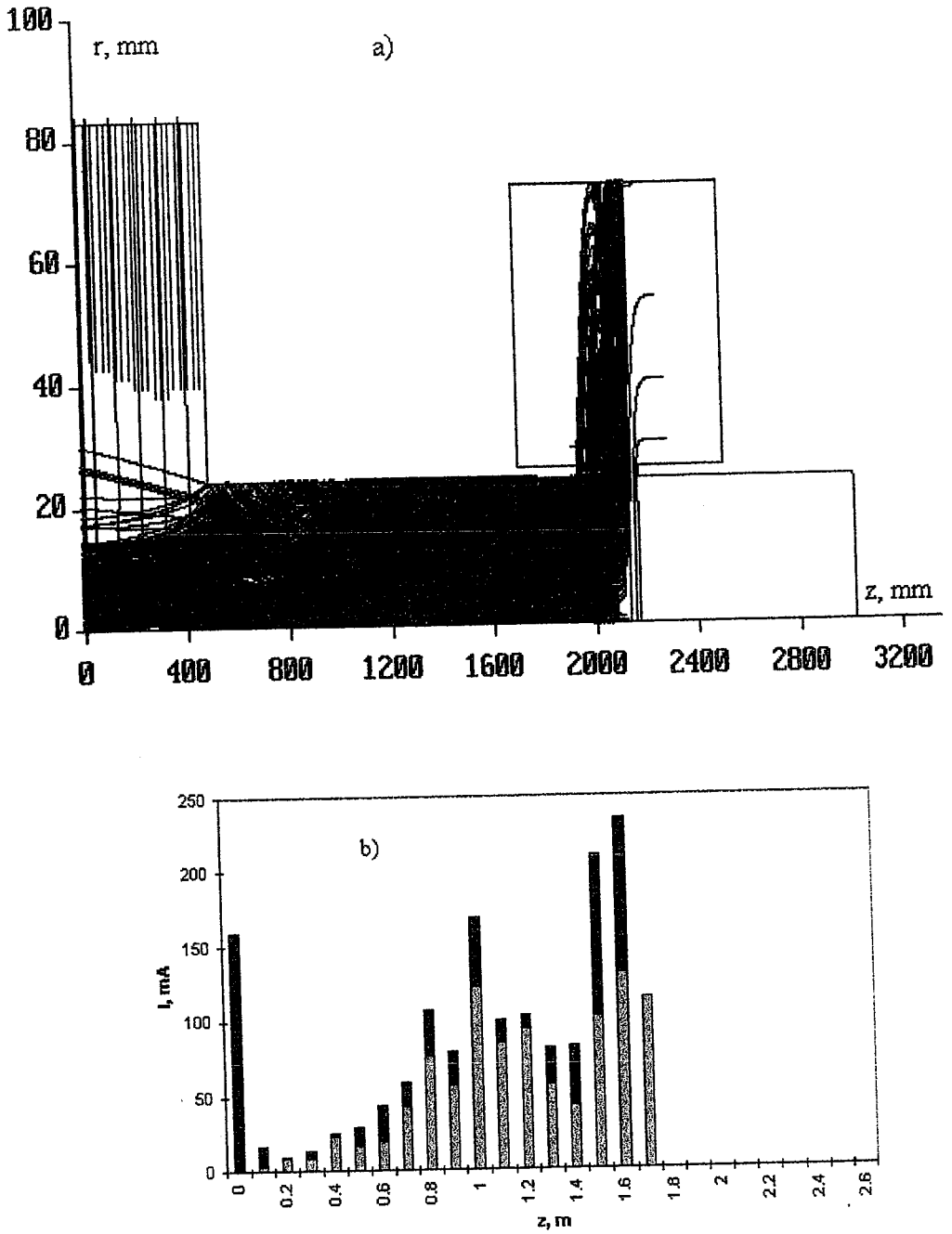

Fig.36. Beam ray trajectories (a) and histogram for prime (lower part of the each column) and backscattered (upper part) beam longitudinal distribution for U(CT1)=75kV, U(CT2)= -60kV. Left column (position z=0) is the beam current which moves into the decelerator in opposite direction.